

Copy

92

RM A9K02

NACA RM A9K02

A9K02

TECH LIBRARY KAFB, NM

0142959



~~CONFIDENTIAL~~
NACA

RESEARCH MEMORANDUM

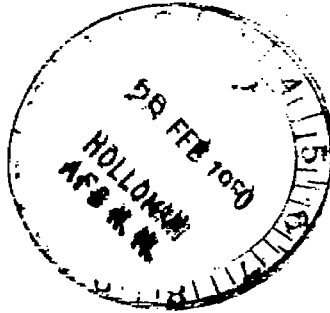
INVESTIGATION OF DOWNWASH AND WAKE CHARACTERISTICS AT
A MACH NUMBER OF 1.53. III - SWEPT WINGS

By Edward W. Perkins and Thomas N. Canning

Ames Aeronautical Laboratory
Moffett Field, Calif.

~~CONFIDENTIAL~~
CLASSIFIED DOCUMENT

This document contains classified information
pertaining to the National Defense of the United
States. It is the intent of the Espionage Act,
USC Section 793, that the transmission or the
revelation of its contents in any manner to an
unauthorized person shall be prohibited by law.
Information so contained may be imparted
only to persons in the armed forces and naval
services of the United States, and to civilian
officers and employees of the Federal Government
who have a legitimate interest in it, and to
United States citizens who have been lawfully
and discretion who of necessity must be
informed thereof.



**NATIONAL ADVISORY COMMITTEE
FOR AERONAUTICS**

WASHINGTON
February 23, 1950

~~CONFIDENTIAL~~

319.98/13



0142959

NACA RM A9K02

NATIONAL ADVISORY COMMITTEE FOR AERONAUTICS

RESEARCH MEMORANDUMINVESTIGATION OF DOWNWASH AND WAKE CHARACTERISTICS AT
A MACH NUMBER OF 1.53. III - SWEPT WINGS

By Edward W. Perkins and Thomas N. Canning

SUMMARY

The results of an experimental investigation of the downwash and wake characteristics behind two highly swept wings in a supersonic stream are presented. The leading-edge sweep angles of the two wings were 63° and $63^{\circ}45'$, the aspect ratios were 3.50 and 1.66, and the corresponding taper ratios were 0.25 and 1.00. The Mach number of the tests was 1.53 and the Reynolds numbers based on the mean aerodynamic chords were 1.4 million for the tapered wing and 2.6 million for the untapered wing. Measurements were made of the variation of downwash angle with angle of attack at several positions within the induced flow field. Additional surveys were made to determine the position and extent of the friction wake. The experimental downwash results were compared with the characteristics calculated by means of the linear theory.

Agreement between the experimental and theoretical values of the rate of change of downwash angle with angle of attack at zero lift was good only at isolated points. In general, the experimental values for the tapered wing were much less than the theoretical. At most of the survey points the rate of change of downwash angle with angle of attack for the tapered wing did not exceed, at any angle of attack, the corresponding theoretical values of the rate of change of downwash at zero lift. The differences between the experimental results for the untapered wing and the theoretical calculations are believed to result from differences between the actual load distribution and that calculated by theory.

The general characteristics of the friction wake were similar to those observed in subsonic flow. With increasing distance downstream from the trailing edge the wake expanded and, with the wing at positive angles of attack, moved downward relative to the free-stream direction. In general, the maximum pitot-pressure loss at the wake center line decreased with increasing distance behind the trailing edge.

INTRODUCTION

A complete theoretical determination of the longitudinal stability characteristics of supersonic aircraft requires a knowledge of the

distribution of downwash and of the characteristics of the friction wake. Theoretical methods for predicting the variation of the downwash angle with angle of attack at zero lift for bodies of revolution and for lifting surfaces of a wide variety of plan forms are available (references 1, 2, and 3). However, for the case of finite lift no theoretical methods for predicting the effects on the downwash distribution of either the rolling up of the vortex sheet or of the presence of the friction wake are now available.

In order to determine the reliability and limits of applicability of the theoretical methods for predicting downwash distribution and to gain some insight into the effects of the friction wake and of the rolling up of the vortex sheet, an experimental investigation of the downwash and wake characteristics for several wing plan forms was undertaken. The first two reports of the investigation (references 4 and 5) dealt with the results for a rectangular and a triangular plan-form wing; the present report is concerned with the downwash and wake characteristics of two highly swept wings.

SYMBOLS

- a slope of any ray through the origin divided by slope of the Mach lines
- c local chord, inches
- c_o root chord, inches
- c_t tip chord, inches
- C_L lift coefficient
- C_N normal-force coefficient
- H free-stream total pressure, pounds per square inch
- ΔH^* difference between the pitot pressure at a point in the wake and the pitot pressure in the free stream where the pitot pressure is the pressure measured by a pitot tube in either subsonic flow, where this pressure is the local total pressure, or in supersonic flow where this pressure is equal to the local total pressure for the flow behind a normal shock wave, pounds per square inch
- m slope of leading edge divided by slope of the Mach lines
$$\left(\beta \cot \Lambda_{L.E.} \right)$$

m_t	slope of the trailing edge divided by slope of the Mach lines $(\beta \cot \Lambda_{T.E.})$
M	free-stream Mach number
P_L	pressure at a point on the lower surface of the wing, pounds per square inch
P_U	pressure acting at a point on the upper surface of the wing, pounds per square inch
q	free-stream dynamic pressure, pounds per square inch
R	Reynolds number
s	semispan, inches
u	perturbation velocities in the x direction
u_a	value of u_Δ at any value of a
u_0	value of u_Δ at $a=0$ for wing with subsonic leading edge
u_Δ	basic perturbation velocity as given by solution for the triangular wing with subsonic leading edge $\left[\frac{\alpha V m^2}{\beta E(k') \sqrt{m^2 - a^2}} \right]$
V	free-stream velocity, feet per second
w	perturbation velocities in the z direction
x, y, z	longitudinal, lateral, and normal coordinates, respectively, with the origin at the leading-edge apex of the wing and the x axis corresponding to the free-stream direction
$E(k')$	complete elliptic integral of the second kind with modulus k'
$F(\phi, k)$	incomplete elliptic integral of the first kind with modulus k and sin amplitude ϕ
$K(k)$	complete elliptic integral of the first kind with modulus k
α	angle of attack, degrees
α_t	angle of twist relative to root chord, degrees
β	$\sqrt{M^2 - 1}$

ϵ	downwash angle measured from the free-stream direction, degrees
ϵ'	difference between the downwash angle at angle of attack and the downwash angle at $\alpha = 0$, degrees
$(\frac{d\epsilon'}{d\alpha})_{L=0}$	rate of change of downwash angle with angle of attack at zero lift
ζ	$y + iz$ $x + \sqrt{x^2 - \beta^2 y^2 - \beta^2 z^2}$, complex argument for the solution of the supersonic flow equations
$\Lambda_{L.E.}$	sweepback angle of leading edge
$\Lambda_{T.E.}$	sweepback angle of trailing edge
r.p.	real part of a complex variable

APPARATUS AND TESTS

The tests were performed in the Ames 1- by 3-foot supersonic wind tunnel No. 1. During this investigation the wind tunnel, which is a variable-pressure closed-return wind tunnel, was equipped with a fixed nozzle which gave a test section Mach number of 1.53.

Detailed drawings giving the pertinent dimensions of the two semispan models and of the support system used in this investigation are shown in figures 1 and 2. Model A had a leading-edge sweep angle of 63° , an aspect ratio of 3.5, and a taper ratio of 0.25. The airfoil sections parallel to the free-stream direction had an NACA 64A005 thickness distribution and the wing was cambered and twisted to give, theoretically, a uniform load distribution at the design lift coefficient of 0.25 at $M=1.5$. (See references 6 and 7.) Model B, which was not twisted, had a leading-edge sweep angle of $63^\circ 45'$, an aspect ratio of 1.66, and a taper ratio of 1.0. The airfoil sections normal to the leading edge were symmetrical, biconvex, circular-arc sections, 15.9 percent thick. This large thickness ratio resulted from the use of 7-percent-thick sections in the streamwise direction. This choice was based on model strength considerations since the same model was used in pressure-distribution tests (reference 8).

The orientation of the models, of the boundary-layer plate, and of the survey stations is shown in figure 2. A detailed description of the support system and a discussion of the precautions taken to minimize the disturbances in the tunnel air stream caused by the boundary-layer plate are given in reference 4. The necessity of using a boundary-layer plate in conjunction with these tests limited the extent of the flow field downstream of the models that was free of disturbances from the plate. Consequently, most of the downwash survey stations, particularly for model B, are not sufficiently far behind the wing to be in likely tail positions. The locations of the downwash survey points relative to the pertinent Mach cones for models A and B are shown in figure 3.

The experimental procedure used in this investigation was the same as that described in reference 4, which is part I of this series of reports. The downwash angles at each survey point were measured by the use of a small cone. For each angle of attack of the model, the angle of attack of the cone was adjusted until the pressures on the upper and lower surfaces were equalized. The resulting angle of attack of the cone was the local stream angle. Except where specifically noted, all details of model construction and support, instrumentation, and reduction and correction of data are identical to those described in reference 4. The test Reynolds numbers based on the mean aerodynamic chords were 1.4 million for the tapered wing and 2.6 million for the untapered wing. For continuity in this series of reports and to aid in the reduction of the data, the same numbering system for the downwash and wake-survey stations that was used in references 4 and 5 has been retained.

CORRECTIONS AND PRECISION

The downwash angles presented for survey stations 2 and 4 were corrected by superposition of the stream deflections caused by both the support system and the nonuniformity of the free stream. The data for station 3 have not been corrected for these interference effects since no suitable stream calibration was obtained at this station. However, in view of the relative positions of stations 2 and 3, it is believed that at station 3 these interference effects were only slightly greater than at station 2. Since the corrections at station 2 were small and had little effect on the final results, it is believed that the uncorrected results presented for station 3 are at least qualitatively useful.

The precision of the results presented is the same as that of reference 4. The experimental values of ϵ' and α are accurate to within $\pm 0.1^\circ$ and $\pm 0.05^\circ$, respectively. The locations of the viscous wake boundaries, which have been taken as the points at which $\frac{\Delta H}{H} = -0.005$, are correct to within 0.06 inch. This is 1.9 percent of the mean aerodynamic chord of model A and 1.0 percent of the mean aerodynamic chord of model B.

THEORETICAL CONSIDERATIONS

The linearized theory of compressible flow has been used to compute the lift distributions for a wide variety of wing plan forms. The two most common approaches used are the conical-flow superposition method and the doublet distribution method. Either method may be used to calculate the load distribution over a given plan form. Since, for linearized flow solutions, there is a unique relationship between the loading and the downwash perturbation velocity w , the downwash field corresponding to any given lift distribution can be calculated. The lift distribution for wing plan forms with both leading and trailing edges swept behind their respective Mach lines has been investigated in reference 9 by the use of the conical-flow superposition method; but no treatment of the corresponding downwash field has as yet been published.

In reference 9, the superposition of linearized conical flows is used to form a finite wing from a flat lifting triangle of infinite chord by cancellation of the lift behind the lines which are to form the trailing edge and outboard of the lines forming the tips. The lift cancellation at the wing boundaries is achieved by a superposition of uniformly loaded lifting elements. The linearized solution for the flow field of these elements is conical with respect to the apex of each element. In reference 9, expressions for the distribution of the streamwise perturbation velocity u of these elements were derived and used in the investigation of the lift distribution.

At first glance it would appear that the procedure used in reference 9 for calculation of the lift distribution could be applied directly to the determination of the entire downwash field. However, in the treatment of the lift problem certain difficulties were encountered in satisfying the boundary conditions within the region influenced by the wing tips and certain approximations for the treatment of the lift problem were necessary. Although these approximations do not satisfy the requirement of zero pressure difference off the wing, they are satisfactory in the treatment of the total lift problem since the area of the lifting surface affected is usually small. These approximations are, however, unsatisfactory for the calculation of downwash distribution in the region influenced by the wing tips. Furthermore, it is apparent from the results of recent experimental investigations (references 8 and 10) of the pressure distributions for models A and B that the linear theory does not predict adequately the lifting pressure distribution in the region affected by the trailing edge and tip. The poor agreement within the Mach cone from the trailing-edge apex has been attributed primarily to viscous effects which are not considered in the theory. Near the tip the failure of the theory is believed to be due both to viscous effects and to the effects of distortion of the discharged vortex sheet at the tip. In view of both the theoretical considerations and the experimental results, therefore, it appears unlikely that anything would be gained by further attempts to calculate the downwash distribution in the region influenced by the wing tips until a more suitable method of predicting the load distribution within this region becomes available.

Although the load distribution in the region influenced by the trailing edge is known to differ from that predicted by the linear theory, the difference is generally less than in the region influenced by both the tip and trailing edge. Therefore, since the downwash distribution in that part of the induced flow field that is not influenced by the tip can be determined within the limitations of the linear theory, calculations for that part of the flow field have been performed. The general procedure for calculating the downwash field within this region is to start with the solution for a flat lifting triangle of infinite chord having the same ratio of the tangents of the leading-edge half-apex angle and Mach angle as the wing under consideration. This solution is conical with respect to the leading apex. Charts of the downwash field for a series of such lifting surfaces are available in reference 11. Cases not specifically

calculated may be determined by interpolation of these results. The equation for the spanwise distribution of velocity to be canceled in the formation of the trailing edge is given in reference 12 for the triangular wing of infinite chord and, in the notation of this paper, is

$$u_{\Delta} = \frac{\alpha V m^2}{\beta E(k^*) \sqrt{m^2 - a^2}} \quad (1)$$

The cancellation of the pressures represented by this velocity distribution is accomplished by the use of two primary elements. A symmetrical trailing-edge element is used to cancel the major portion of the pressure behind the trailing edge. The expression for the downwash component w associated with this element has been derived in the appendix and is

$$w = r.p. \frac{-u_0}{K(k)} \frac{1}{m_t} \cosh^{-1} \frac{1}{2} \left[\sqrt{(1+m_t y_0^*)^2 + m_t^2 z_0^*} + \sqrt{(1-m_t y_0^*)^2 + m_t^2 z_0^*} \right] \quad (2)$$

where

$$y_0^* = \frac{y_0/x_0}{1-(z_0/x_0)^2} \quad z_0^* = \frac{-(z_0/x_0)\sqrt{1-(y_0/x_0)^2-(z_0/x_0)^2}}{1-(z_0/x_0)^2}$$

where

$$x_0 = x - c_0 \quad y_0 = \beta y \quad z_0 = \beta z$$

$$u_0 = \frac{m V \alpha}{\beta E(k^*)} \quad (\text{value of } u_{\Delta} \text{ at } a=0) \quad (3)$$

The cancellation of the remainder of the pressure at the trailing edge is achieved by a superposition of oblique trailing-edge elements. The expression for the downwash component w associated with the oblique trailing-edge elements, as derived in the appendix, is

$$w = r.p. \frac{u_a}{2\pi a} \left[\sqrt{1-a^2} \log \frac{(\sqrt{1+a} \Omega - \sqrt{m_t - a} \Phi)^2 + (\sqrt{1+a} X - \sqrt{m_t - a} \Theta)^2}{(\sqrt{1+a} \Omega + \sqrt{m_t - a} \Phi)^2 + (\sqrt{1+a} X + \sqrt{m_t - a} \Theta)^2} \right. \\ \left. \sqrt{\frac{(m_t - a)(1 - a)}{m_t}} \log \frac{(\Omega - \sqrt{m_t} \Phi)^2 + (X - \sqrt{m_t} \Theta)^2}{(\Omega + \sqrt{m_t} \Phi)^2 + (X + \sqrt{m_t} \Theta)^2} \right] \quad (4)$$

where

$$\Omega = \sqrt{\frac{w + (m_t - y_a^*)}{2}}$$

$$\Theta = \sqrt{\frac{\psi - (1+y_a^*)}{2}}$$

$$\Phi = \sqrt{\frac{\psi + (1+y_a^*)}{2}}$$

$$\omega = \sqrt{(m_t - y_a^*)^2 + z_a^*{}^2}$$

$$X = \sqrt{\frac{w - (m_t - y_a^*)}{2}}$$

$$\psi = \sqrt{(1+y_a^*)^2 + z_a^*{}^2}$$

where

$$y_a^* = \frac{y_a/x_a}{1 - (z_a/x_a)^2}$$

$$z_a^* = \frac{-(z_a/x_a) \sqrt{1 - (y_a/x_a)^2 - (z_a/x_a)^2}}{1 - (z_a/x_a)^2}$$

The expression for the contribution of all the oblique trailing-edge elements superimposed along the trailing edge from $a=0$ to $a=a_0$ is

$$\left(\frac{w}{\alpha V} \right)_{x,y,z} = - \frac{1}{2\pi\beta E(k') m} \int_0^{a_0} \frac{1}{[1 - (a/m)^2]^{3/2}} \left[\begin{aligned} & \sqrt{1-a^2} \log \frac{(\sqrt{1+a}\Omega - \sqrt{m_t-a}\Phi)^2 + (\sqrt{1+a}X - \sqrt{m_t-a}\Theta)^2}{(\sqrt{1+a}\Omega + \sqrt{m_t-a}\Phi)^2 + (\sqrt{1+a}X + \sqrt{m_t-a}\Theta)^2} - \\ & \sqrt{\frac{(m_t-a)(1-a)}{m_t}} \log \frac{(\Omega - \sqrt{m_t}\Phi)^2 + (X - \sqrt{m_t}\Theta)^2}{(\Omega + \sqrt{m_t}\Phi)^2 + (X + \sqrt{m_t}\Theta)^2} \end{aligned} \right] da \quad (5)$$

where a_0 is either the value of a at the point of intersection of the trailing edge and the Mach cone from the leading-edge tip or the value of a for the most rearward element that will influence the point x,y,z . In the first instance,

$$a_0 = \frac{\beta y}{x} = m_t \left(1 - \frac{c_0}{x} \right) \quad (6)$$

where

$$x = \frac{\beta s \left(1 + \frac{1}{m} \right) + m_t c_0}{1 + m_t}$$

In the second instance, the expression is

$$a_0 = \frac{-B - \sqrt{B^2 - 4AC}}{2A} \quad (7)$$

where

$$A = x^2 - \beta^2 z^2 - (m_t c_0 + \beta y)^2$$

$$B = 2m_t [x(c_0 - x) + \beta y(m_t c_0 + \beta y) + \beta^2 z^2]$$

$$C = m_t^2 [(x - c_0)^2 - \beta^2(y^2 + z^2)]$$

The evaluation of equation (5) between the limits $a=0$ to $a=a_0$ for any point x, y, z gives the contribution of the oblique trailing-edge elements for cancellation of lift behind the right half of the wing. The contribution of the oblique elements for the other half-wing is most easily determined by making use of equation (5) with the sign of y reversed. The upper limit of integration is, of course, changed since a_0 is also a function of y .

The total theoretical value of $(d\epsilon/d\alpha)_{L=0}$ at any point x, y, z which is not in the Mach cone from the leading-edge tip (fig. 3) is then the sum of three solutions: first, the contribution of the basic solution obtained from reference 11; second, the contribution of the symmetrical trailing-edge element (equation (2)); and, third, the contribution of the oblique trailing-edge elements (equation (5) evaluated for both positive and negative values of y). Calculations of the theoretical downwash distribution have been made for models A and B for comparison with the experimental results in the region not influenced by the wing tip. These results are presented in table I.

RESULTS AND DISCUSSION

Rate of Change of Downwash with Angle of Attack at Zero Lift

The variation of downwash angle with angle of attack at each survey point for models A and B are presented in figures 4 and 5, respectively. The theoretical values of $(d\epsilon/d\alpha)_{L=0}$ are also shown for all survey points which are not within the Mach cones from the leading-edge tips (fig. 3). For model A, the straight lines representing these theoretical values have been drawn through the experimental curves at $\alpha = 1.2^\circ$ for comparison with the experimental results. This was done since the force tests of reference 7 showed that the angle of zero lift for model A was approximately 1.2° . (See fig. 6.) For model B, the angle of zero lift has been assumed to be zero angle of attack, as in reference 8, since the airfoil sections were symmetrical about the chord plane.

The experimental and theoretical values of $(d\epsilon/d\alpha)_{L=0}$ agree only at isolated points for both models (the 30-, 40-, and 50-percent semispan positions at station 2, and the 10- and 30-percent positions at station 4 for model A; the 10-, 70-, and 90-percent semispan positions at station 2, and the 10-percent semispan position at station 4 for model B). For all the remaining survey positions for both models, the experimental values of $(d\epsilon'/d\alpha)_{L=0}$ were less than the theoretical values. Based on the results presented in figure 6 a somewhat smaller difference might be anticipated since, in the low angle-of-attack range, the experimental lift and normal force-curve slopes for models A and B, respectively, are only slightly less than that predicted by theory. More recent experimental results for model A (reference 13) show that the lift-curve slope is a function of Reynolds number and that, at a Reynolds number of 1.5×10^6 which is approximately the Reynolds number for the downwash tests, the value of the lift-curve slope is 0.049 per degree as against 0.044 per degree shown in figure 6. Both of these experimental values are only slightly less than the theoretical value of 0.051 per degree.

Variation of Downwash Angle with Angle of Attack

The slopes of the experimental curves which describe the variation of downwash with angle of attack for model A (fig. 4) did not exceed, at any angle of attack, the corresponding theoretical values of $(d\epsilon/d\alpha)_{L=0}$ except at the 80- and 90-percent semispan positions at station 2 and the 5-percent semispan position at stations 2 and 3. The 80- and 90-percent semispan positions at station 2 were near the position of the disturbance from the apex of the trailing edge. (See fig. 3.) Since the instrument used for measuring the stream angles will not function properly in a region of large pressure gradient, it may not have indicated accurately the stream angles near the disturbance from the trailing-edge apex. The 5-percent semispan position was, of course, very close to the boundary-layer plate and, as will be shown later, the thickness and intensity of the friction wake behind the wing and close to the boundary-layer plate were disproportionately large. Hence, it is probable that the downwash at this point was influenced by the interference between the model and the boundary-layer plate.

Since the downwash at any point in the induced flow field depends on the lift distribution within the Mach forecone of the point, it is possible to study the relation between the variation with angle of attack of the downwash and lift, provided sufficient correlative data are available. In order to be able to correlate the data, the downwash survey point must be so located relative to the wing that the Mach forecone of the point includes only an area of the wing wherein a detailed knowledge of the load distribution is available. For model A the downwash survey points are located so far downstream relative to the wing that almost the entire wing is included within the Mach forecone from any of the survey points. Consequently, the downwash at each survey point is affected by the variation of lift

distribution over most of the wing. Hence, to obtain any correlation between downwash and lift for this wing, a detailed knowledge of the variation of wing loading with angle of attack over the entire wing would be required. The load distributions given in reference 10 for model A are insufficient for this study. However, for model B, at least a qualitative correlation is possible since a proportionately smaller part of this wing affects the downwash at survey station 2.

Figure 7 shows the theoretical and experimental chordwise distribution of lifting-pressure coefficient per degree angle of attack for five spanwise stations of model B. A typical trace of the Mach forecone on the equivalent flat-plate wing at $\alpha = 0^\circ$ is shown in figure 8. Although the area of the wing included within the Mach forecone varies with angle of attack, this variation is negligible for the angle-of-attack range considered. The chordwise pressure distribution at the 6.4-percent semispan station shows that, at low angles of attack, the lift over the forward portion of the chord is considerably higher than the theoretical. With increasing angle of attack, the pressure-distribution data indicate a sharp decrease in the section lift-curve slope. Between $\alpha = 6^\circ$ and $\alpha = 10^\circ$, the section lift-curve slope would be approximately equal to the theoretical value since the pressure distributions closely approximate the theoretical. The data for the 25.6- and 51.2-percent semispan stations show that, within the region included in the Mach forecone from the 10-percent semispan position, the values of the lifting-pressure coefficients per degree angle of attack generally increase with angle of attack, indicating an increase in the section lift-curve slopes with increasing angle of attack.

At station 2, the effect of these changes in lift distribution is apparent in the variation of downwash with angle of attack at the 10-percent semispan position. The decrease in $d\epsilon'/d\alpha$ which occurs between $\alpha = 2.5^\circ$ and $\alpha = 7^\circ$ is coincident with the decrease in the slope of the section lift curve at the 6.4-percent semispan station. The apparent increase in $d\epsilon/d\alpha$, which accompanies further increases in angle of attack, may be either the result of the increase in section lift-curve slope indicated by the pressure-distribution data for the 6.4-, 25.6- and 51.2-percent semispan stations or the effect of the displacement of the vortex sheet. (See reference 4.) The increase in $d\epsilon'/d\alpha$ with increasing angle of attack at the 30- and 50-percent semispan positions may be due to the increase in lift-curve slope for the portion of the wing included within the Mach forecones from these points. The downwash curve for the 70-percent semispan position exhibits a relatively uniform variation of downwash angle with angle of attack over most of the angle-of-attack range, with a decrease in slope occurring at the higher angles of attack. This decrease is probably associated with the decrease in the lifting pressure coefficient per degree angle of attack which occurs at the higher angles of attack for the region near the leading edge of the wing at the 51.2- and 76.9-percent semispan stations and is particularly apparent at this latter station. Little can be said about the variation of ϵ with α at the 90-percent semispan position, except that it is probably affected to a large

degree by the leading-edge separation which is known to occur on this wing.

A similar correlation of the variation of downwash and load distribution with angle of attack for the data at station 4 is not possible, since the effects of the variation of load distribution within the larger regions of influence for each survey point cannot be determined readily from the available data. As shown in references 4 and 5, an additional factor which would have to be considered, at least for those survey positions some distance behind the wing trailing edge, is the effect of displacement of the vortex sheet on the downwash distribution.

Wake

The pitot-pressure profiles presented in figures 9 and 10 indicate the location, thickness, and intensity of the friction wake for several semispan positions at stations 5 and 6 for models A and B. The data show that, with increasing distance downstream, the wake expanded, and, with the wing at positive angles of attack, moved downward relative to the free stream. In general, the maximum pitot-pressure loss at the wake center line decreased with increasing distance downstream from the trailing edge. An exception is noted at the 30-percent semispan position for model B at station 6. The data indicate slight increases in pitot-pressure loss at the wake center line between stations 5 and 6 and between the 50- and 30-percent semispan points at station 6. Moving the survey instrument from station 5 to station 6 or moving it from the 50-percent to the 30-percent semispan point at station 6 increases the distance between the survey rake and the airfoil trailing edge so that a decrease, rather than the indicated increase, in wake intensity was anticipated. This apparent discrepancy may arise from the lack of sufficient data to define accurately the profiles of pitot-pressure loss.

The disproportionate thickness and intensity of the wake at the 10-percent semispan points are believed to result from interference between the models and support and would not be expected in the case of an isolated wing. This same phenomenon was noted in wake surveys behind a rectangular and a triangular wing under similar test conditions. (See references 4 and 5.)

To illustrate the rapid displacement of the wake with changes in angle of attack, particularly in the region close to the plane of symmetry, spanwise plots of the position of the upper limit of the wake at stations 5 and 6 are presented in figures 11 and 12. These data show that if a conventional stabilizer is to be used in conjunction with the wing-body combination of reference 7 it should be placed at least 0.22 root-chord length above the body axis if the wake is to pass below it at all angles of attack up to approximately 8° . This result does not include the effects of the fuselage but essentially represents a limit, since the effect of the upwash field of the fuselage would, in most cases, cause the wake to rise even higher above the body axis and thus require that the stabilizer be placed even higher.

CONCLUDING REMARKS

The experimental values of the rate of change of downwash at zero lift agree with the values predicted by means of the linear theory only at isolated points for the two highly swept wings used in this investigation. In most instances the experimental values were less than those predicted by the theory.

The slopes of the experimental downwash curves for the tapered wing did not exceed, at any angle of attack, the corresponding theoretical slopes at zero lift except near the boundary-layer plate and in the region of the disturbance from the apex of the trailing edge. The observed variation of the rate of change of downwash with angle of attack under lifting conditions for the untapered wing can be qualitatively explained on the basis of the variation of the load distribution with angle of attack. Thus, it appears that calculation of the variation of downwash with angle of attack may be feasible once the variation of the load distribution with angle of attack has been accurately determined. Additional factors which must be considered, of course, are the effects of the displacement and distortion of the vortex sheet as well as local effects of the friction wake.

Ames Aeronautical Laboratory,
National Advisory Committee for Aeronautics,
Moffett Field, Calif.

APPENDIX

DETERMINATION OF THE DOWNWASH DISTRIBUTION

FOR THE TRAILING-EDGE ELEMENTS

Symmetrical Trailing-Edge Element

The relation between u and w in the conical field in terms of the complex variable ζ is (See reference 14.)

$$w = -i \int_1^\zeta \frac{\sqrt{1-\zeta^2}}{\zeta} \frac{du}{d\zeta} d\zeta \quad (A1)$$

From reference 9 for the symmetrical trailing-edge element

$$u = r.p. u_0 \frac{F(\phi, k)}{K(k)} \quad (A2)$$

where

$$\varphi = \sin^{-1} \sqrt{\frac{1-\zeta^2}{1-m_t^2}}$$

and

$$k = \sqrt{1-m_t^2}$$

Differentiating equation (A2) with respect to ζ

$$\frac{du}{d\zeta} = \frac{u_0}{K(k)} \frac{1}{\sqrt{(1-\zeta^2)(\zeta^2-m_t^2)}}$$

and substituting the result in equation (A1)

$$\begin{aligned} w &= r.p. \frac{-u_0}{K(k)} \int_1^\zeta \frac{d\zeta}{\zeta \sqrt{m_t^2 - \zeta^2}} \\ &= r.p. \frac{u_0}{K(k)} \frac{1}{m_t} \left(\cosh^{-1} \left| \frac{m_t}{\zeta} \right| \right)_1^\zeta \end{aligned} \quad (A3)$$

The value of u_0 is determined from Stewart's equation for the value of u_Δ at $a = 0$

$$u_\Delta = \frac{\alpha V m^2}{\beta E(k') \sqrt{m^2 - a^2}} \quad k' = \sqrt{1-m^2}$$

and

$$u_0 = \frac{m V \alpha}{\beta E(k')}$$

Substituting these results in equation (A3) and taking the real part with the complex variable $\zeta = y_0^* + i z_0^*$

$$\begin{aligned} \frac{w}{\alpha V} &= \frac{1}{\beta E(k') K(k)} \frac{m}{m_t} \cosh^{-1} \frac{1}{2} \left[\sqrt{(1+m_t y_0^*)^2 + m_t^2 z_0^{*2}} + \right. \\ &\quad \left. \sqrt{(1-m_t y_0^*)^2 + m_t^2 z_0^{*2}} \right] \end{aligned} \quad (A4)$$

where

$$y_0^* = \frac{y_0/x_0}{1 - (z_0/x_0)^2}$$

$$z_0^* = \frac{-(z_0/x_0)\sqrt{1 - (y_0/x_0)^2 - (z_0/x_0)^2}}{1 - (z_0/x_0)^2}$$

$$x_0 = x - c_0$$

$$y_0 = \beta y$$

$$z_0 = \beta z$$

c_0 = root chord

Oblique Trailing-Edge Element

From reference 9 for the oblique trailing-edge element

$$u = r.p. \frac{u_a}{\pi} \cos^{-1} \frac{(1+m_t)(a+\xi) - 2(a\xi + m_t)}{(1-m_t)(\xi-a)} \quad (A5)$$

Differentiating (A5) with respect to ξ

$$\frac{du}{d\xi} = \frac{u_a}{\pi} \frac{\sqrt{(m_t-a)(a-1)}}{(\xi-a) \sqrt{(\xi-m_t)(\xi-1)}}$$

Substituting this result in (A1)

$$iw = r.p. \frac{u_a}{\pi} \sqrt{(m_t-a)(a-1)} \int_1^\xi \frac{\sqrt{1-\xi^2} d\xi}{\xi(\xi-a)\sqrt{(\xi-m)(\xi-1)}}$$

from which

$$w = r.p. \frac{u_a}{\pi a} \left[\sqrt{\frac{(1-a^2)}{m_t}} \log \frac{\sqrt{(1+a)(m_t-\xi)} - \sqrt{(m_t-a)(1+\xi)}}{\sqrt{(1+a)(m_t-\xi)} + \sqrt{(m_t-a)(1+\xi)}} - \right.$$

$$\left. \sqrt{\frac{(m_t-a)(1+a)}{m_t}} \log \frac{\sqrt{(m_t-\xi)} - \sqrt{m_t(1+\xi)}}{\sqrt{(m_t-\xi)} + \sqrt{m_t(1+\xi)}} \right] \quad (A6)$$

Letting the complex variable $\zeta = y_a^* + iz_a^*$ and taking the real part of equation (A6)

$$w = \frac{u_a}{2\pi a} \left[\sqrt{1-a^2} \log \frac{(\sqrt{1+a} \Omega - \sqrt{m_t-a} \Phi)^2 + (\sqrt{1+a} X - \sqrt{m_t-a} \Theta)^2}{(\sqrt{1+a} \Omega + \sqrt{m_t-a} \Phi)^2 + (\sqrt{1+a} X + \sqrt{m_t-a} \Theta)^2} - \right.$$

$$\left. \sqrt{\frac{(m_t-a)(1-a)}{m_t}} \log \frac{(\Omega - \sqrt{m_t} \Phi)^2 + (X - \sqrt{m_t} \Theta)^2}{(\Omega + \sqrt{m_t} \Phi)^2 + (X + \sqrt{m_t} \Theta)^2} \right] \quad (A7)$$

where

$$\Omega = \sqrt{\frac{\omega + (m_t - y_a^*)}{2}}$$

$$\omega = \sqrt{(m_t - y_a^*)^2 + z_a^{*2}}$$

$$\Phi = \sqrt{\frac{\psi + (1+y_a^*)}{2}}$$

$$\psi = \sqrt{(1+y_a^*)^2 + z_a^{*2}}$$

$$X = \sqrt{\frac{\omega - (m_t - y_a^*)}{2}}$$

$$\Theta = \sqrt{\frac{\psi - (1+y_a^*)}{2}}$$

where

$$y_a^* = \frac{y_a/x_a}{1 - (z_a/x_a)^2}$$

$$z_a^* = \frac{-(z_a/x_a) \sqrt{1 - (y_a/x_a)^2 - (z_a/x_a)^2}}{1 - (z_a/x_a)^2}$$

where

$$x_a = x - \frac{m_t c_o}{m_t - a} \quad y_a = \beta y - \frac{m_t c_o a}{m_t - a}$$

$$z_a = \beta z$$

c_o = root chord

REFERENCES

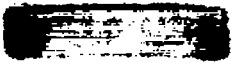
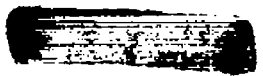
1. Tsien, Hsue-Shen; Supersonic Flow over an Inclined Body of Revolution. *Jour. Aero. Sci.*, vol. V, no. 12, Oct. 1938, pp. 480-483.
2. Lagerstrom, P. A., and Graham, Martha E.: Downwash and Sidewash Induced by Three-Dimensional Lifting Wings in Supersonic Flow. Douglas Aircraft Co., Inc., Rep. No. SM-13007, Apr. 1947.
3. Heaslet, Max. A., and Lomax, Harvard: The Calculation of Downwash Behind Supersonic Wings with an Application to Triangular Plan Forms. NACA TN 1620, 1948.
4. Perkins, Edward W., and Canning, Thomas, N.: Investigation of Downwash and Wake Characteristics at a Mach Number of 1.53. I - Rectangular Wing. NACA RM A8L16, 1949.
5. Perkins, Edward W., and Canning, Thomas, N.: Investigation of Downwash and Wake Characteristics at a Mach Number of 1.53. II - Triangular Wing. NACA RM A9D20, 1949.
6. Jones, Robert T.: Estimated Lift-Drag Ratios at Supersonic Speed. NACA TN 1350, 1947.
7. Madden, Robert T.: Aerodynamic Study of a Wing-Fuselage Combination Employing a Wing Swept Back 63° .- Investigation at a Mach Number of 1.53 to Determine the Effects of Cambering and Twisting the Wing for Uniform Load at a Lift Coefficient of 0.25. NACA RM A9C07, 1949.
8. Boyd, John, W., Katzen, Elliott D., and Frick, Charles W.: Investigation at Supersonic Speed ($M=1.53$) of the Pressure Distribution Over a 63° Swept Airfoil of Biconvex Section at Several Angles of Attack. NACA RM A8F22, 1948.
9. Cohen, D.: The Theoretical Lift of Flat Swept-Back Wings at Supersonic Speeds. NACA TN 1555, 1948.
10. Stephens, Victor I., and Boyd, John W.: A Comparison of Theoretical and Experimental Lifting Pressures on a 63° Swept-Back Wing for Mach Numbers from 1.15 to 1.7 and a Reynolds Number of 4.5 Million. NACA RM A9C16, 1949.
11. Nielsen, Jack N., and Perkins, Edward W.: Charts for the Conical Part of the Downwash Field of Swept Wings at Supersonic Speeds. NACA TN 1780, 1948.
12. Stewart, H. J.: The Lift of a Delta Wing at Supersonic Speeds. *Quart. of Applied Math.*, vol. IV, no. 3, Oct. 1946, pp. 246-254.

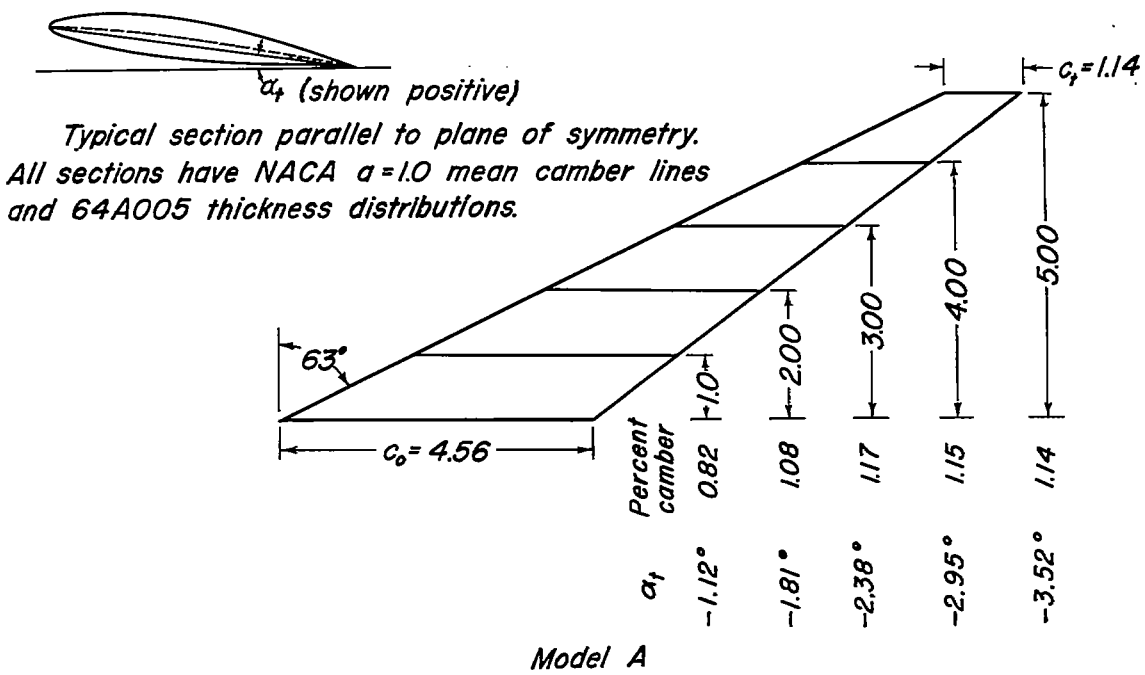
- CONFIDENTIAL
13. Hall, Charles F., and Heitmeyer, John C.: Aerodynamic Study of a Wing-Fuselage Combination Employing a Wing Swept Back 63° .— Characteristics at Supersonic Speeds of a Model with the Wing Twisted and Cambered for Uniform Load. NACA RM A9J24, 1949.
 14. Jones, Robert T.: The Use of Conical and Cylindrical Fields in Supersonic Wing Theory. NACA — University Conference on Aerodynamics: A compilation of the papers presented, Langley Field, Va., June 21-23, 1948, pp. 341-354. (Available from the Durand Reprinting Committee, Cal. Inst. of Tech., Pasadena, Calif.)

TABLE I.— CALCULATED DOWNWASH

Station	$\frac{x}{c}$	$\frac{z}{c}$	$\frac{y}{s}$	Basic conical (reference 11)	Trailing-edge elements		$\left(\frac{de}{d\alpha}\right)_{L=0}$
					Symmetrical (equation (2))	Oblique (equation (5))	
Model A							
2	2.1	0.22	10	0.810	-0.440	0.039	0.409
			20	.801	-.406	.006	.401
			30	.785	-.356	-.026	.403
			40	.770	-.298	-.057	.415
			50	.740	-.237	-.084	.419
			60	.695	-.160	-.092	.443
			70	.610	-.101	-.059	.450
			80	.440	-.030	-.015	.395
			90	.180	---	---	.180
3	2.1	.44	10	.675	-.254	.032	.453
			20	.665	-.240	.008	.433
			30	.652	-.220	-.016	.416
			40	.623	-.190	-.041	.392
			50	.580	-.148	-.043	.389
			60	.510	-.101	-.031	.378
			70	.425	-.049	-.011	.365
			80	.338	---	---	.338
			90	---	---	---	---
4	3.0	.22	10	.860	-.604	.125	.381
			30	.850	-.534	-.018	.298
Model B							
2	1.7	.17	10	.817	-.445	.002	.374
			30	.800	-.252	-.017	.531
			50	.764	-.088	-.003	.673
			70	.673	-.020	-.000	.653
			90	.340	---	---	.340
4	2.4	.17	10	.867	-.675	.029	.221
			20	.860	-.593	.008	.275







All dimensions in inches

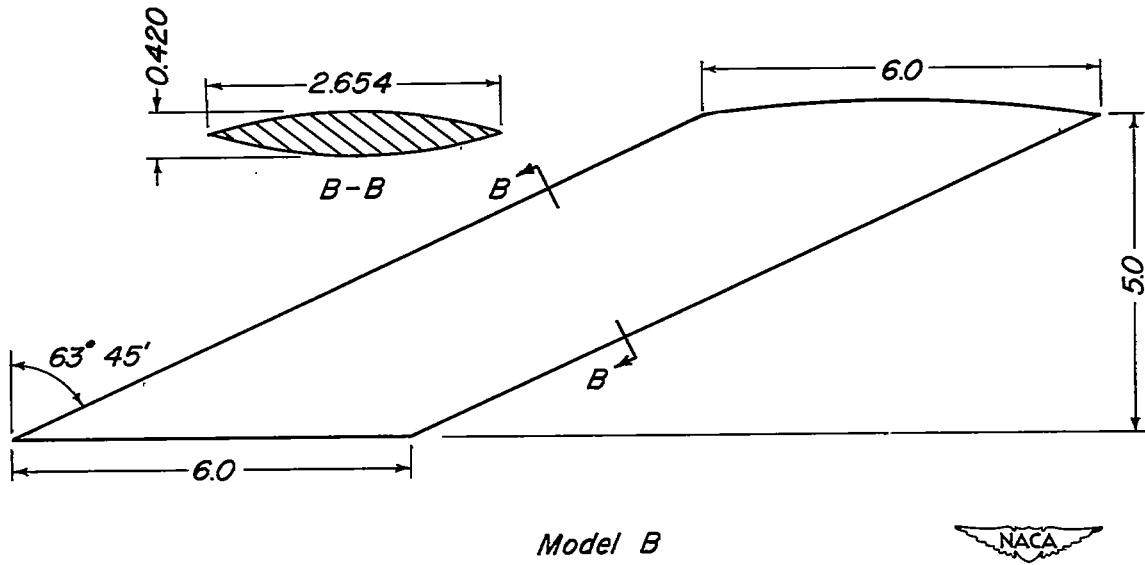


Figure 1.—Sketch of models A and B.

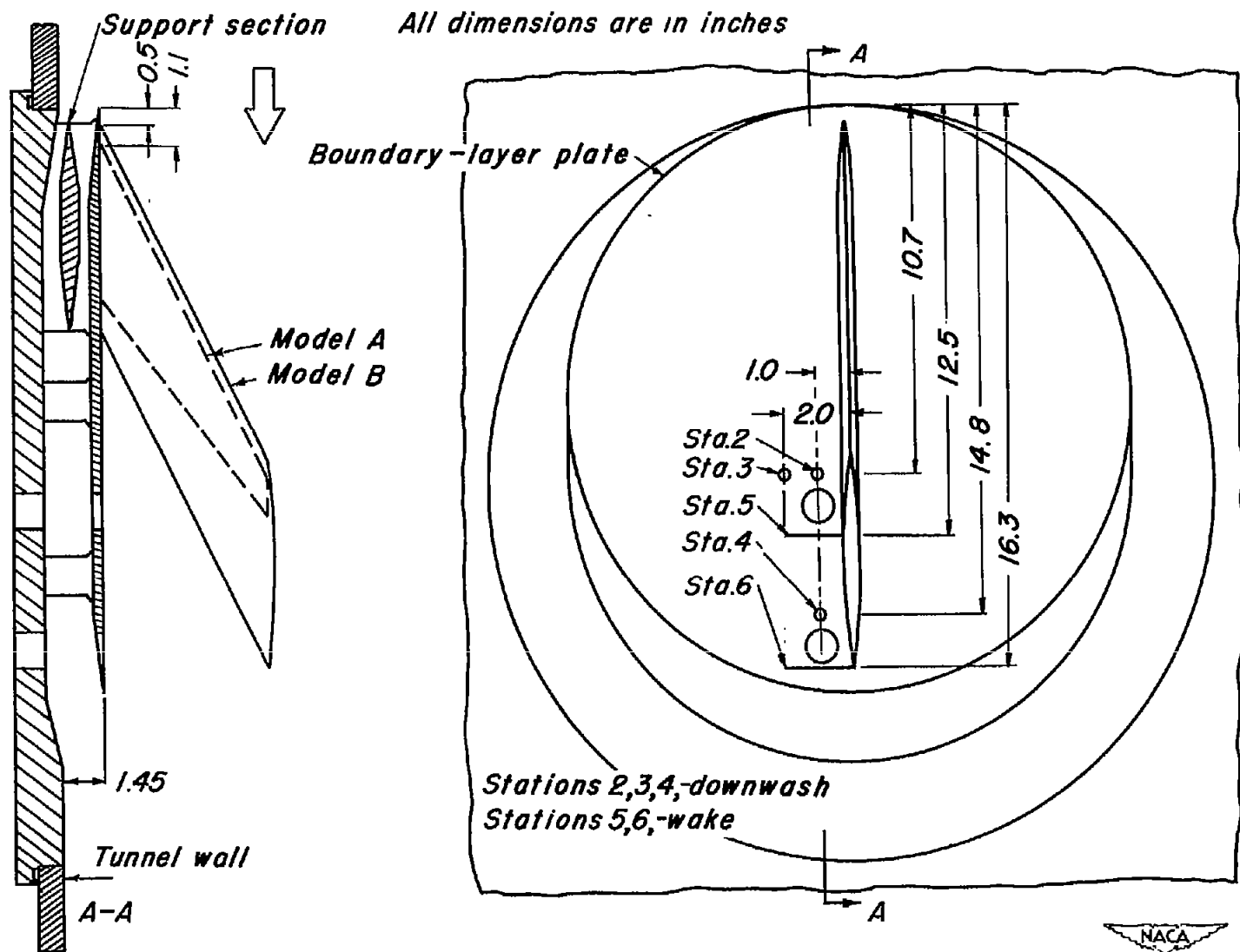


Figure 2.—Sketch of model support system and survey stations.

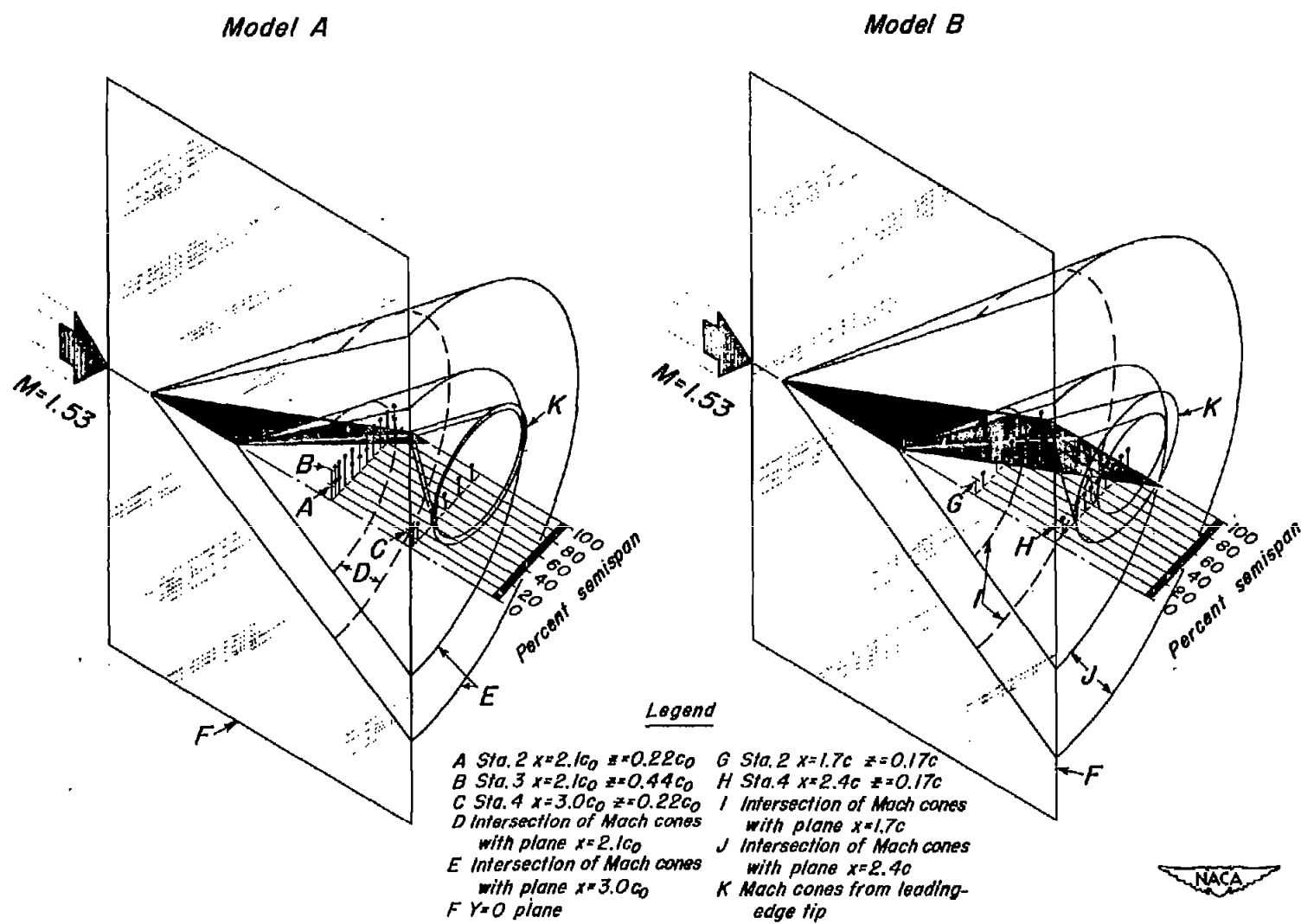


Figure 3.—Sketches showing the locations of the downwash survey stations relative to the Mach cones for models A and B.

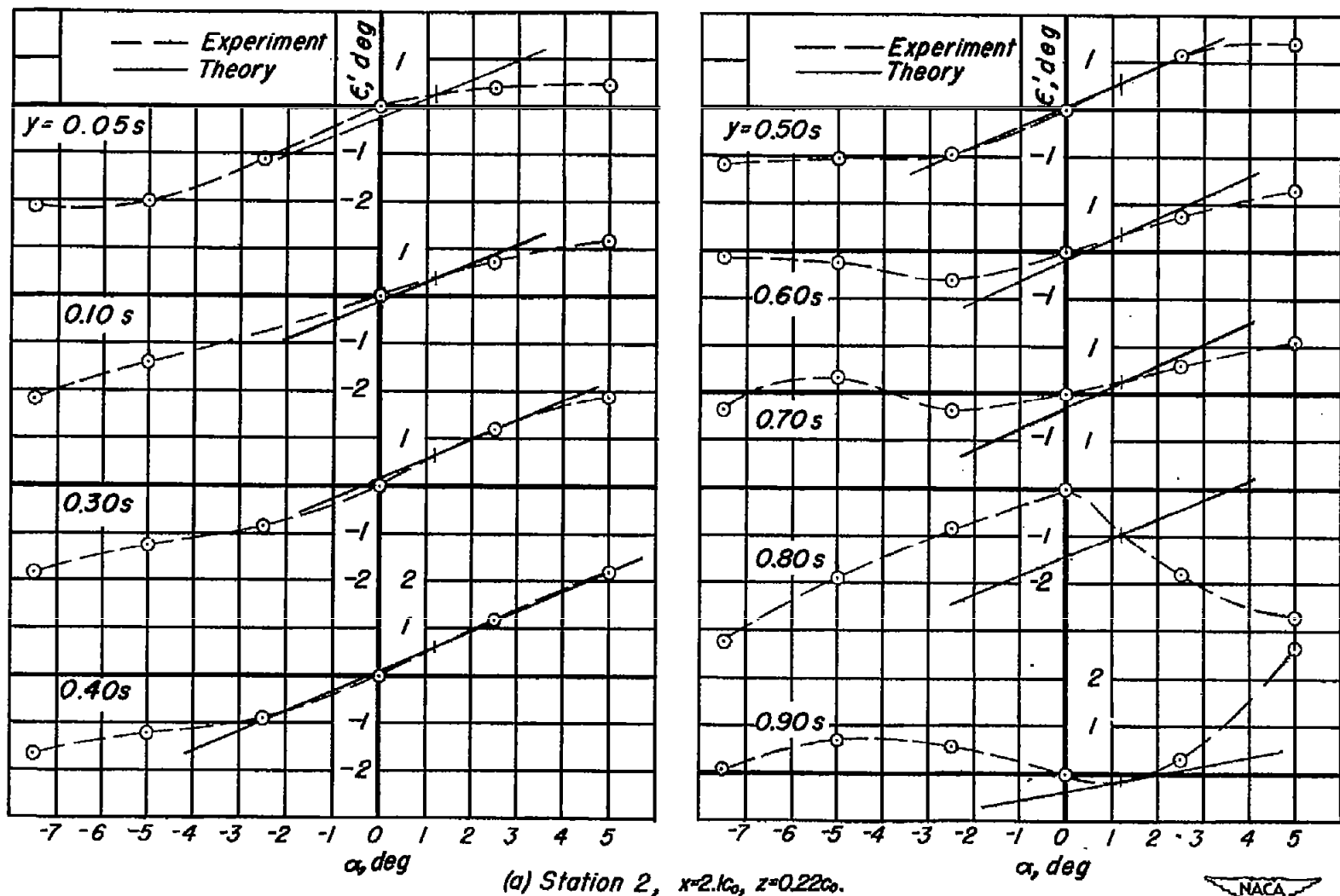


Figure 4. — Variation of downwash angle with angle of attack, Model A.

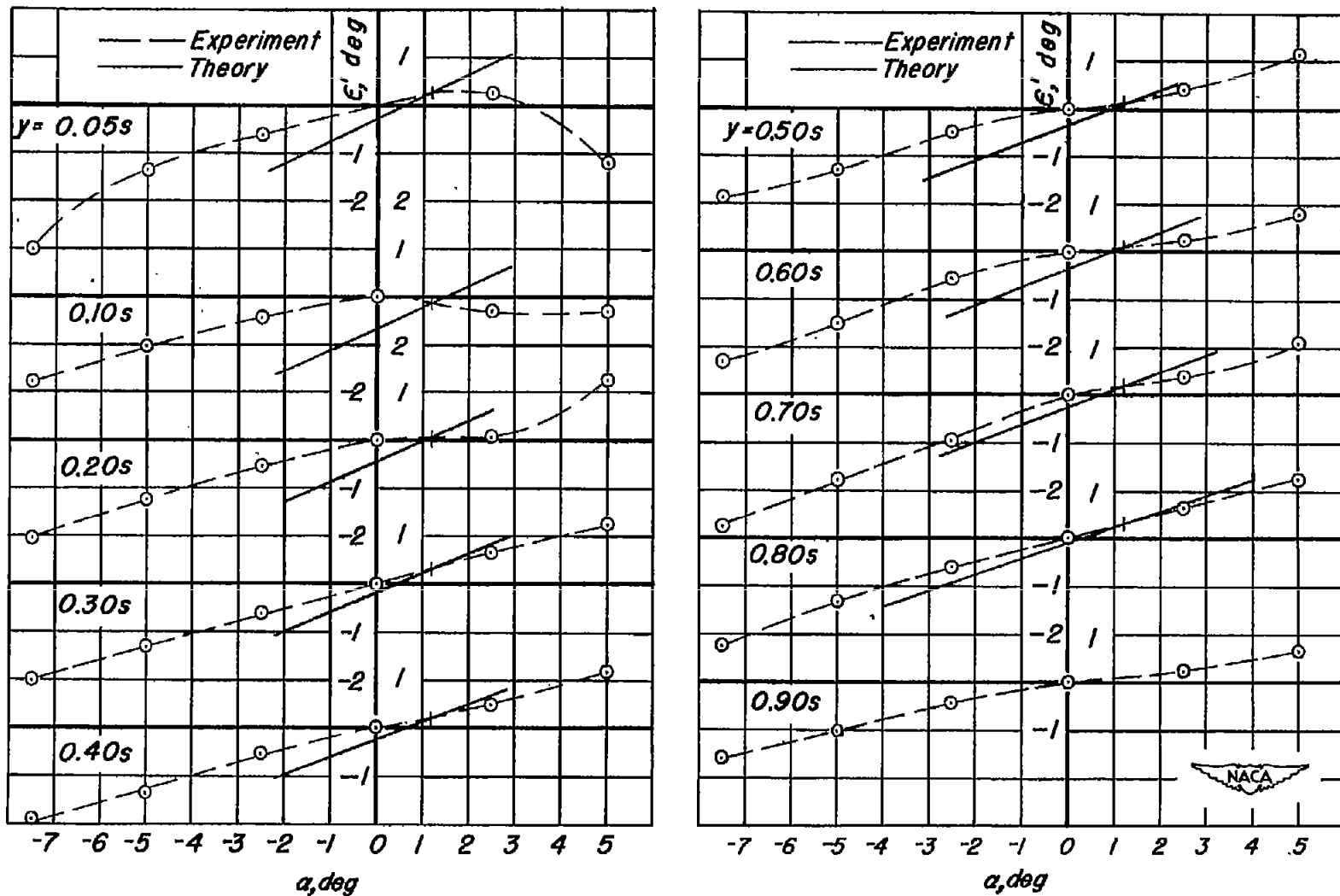


Figure 4.—Continued.

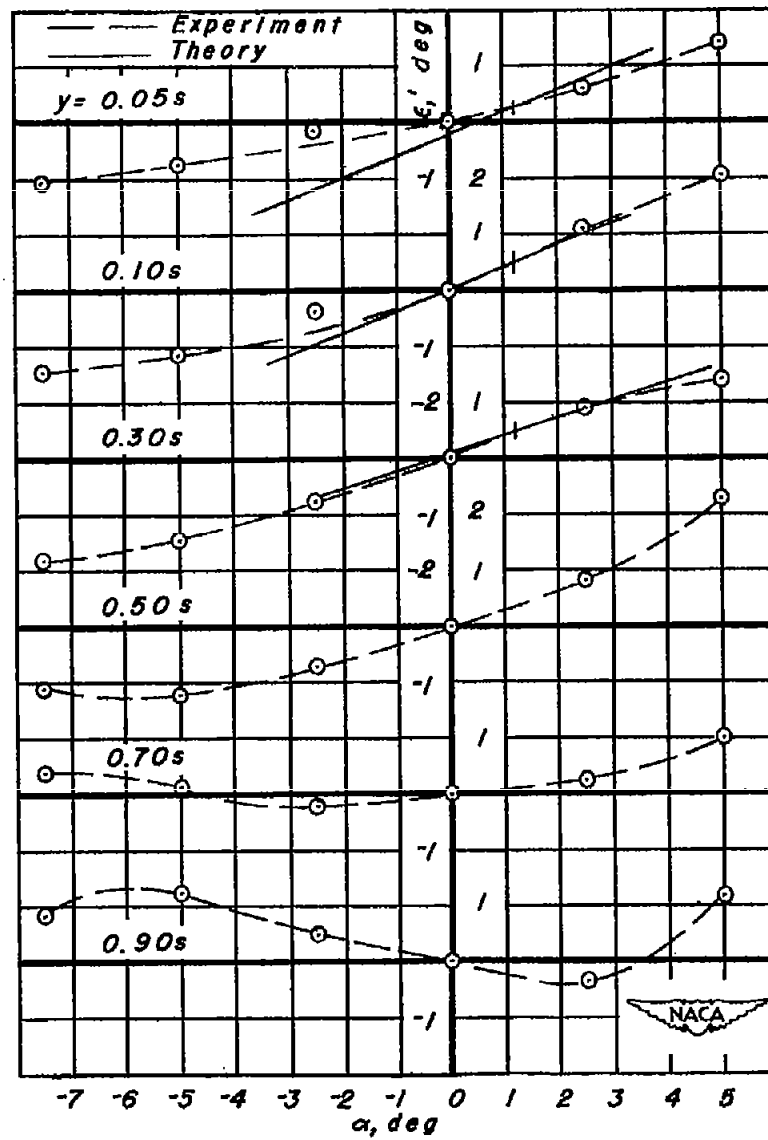


Figure 4. - Concluded

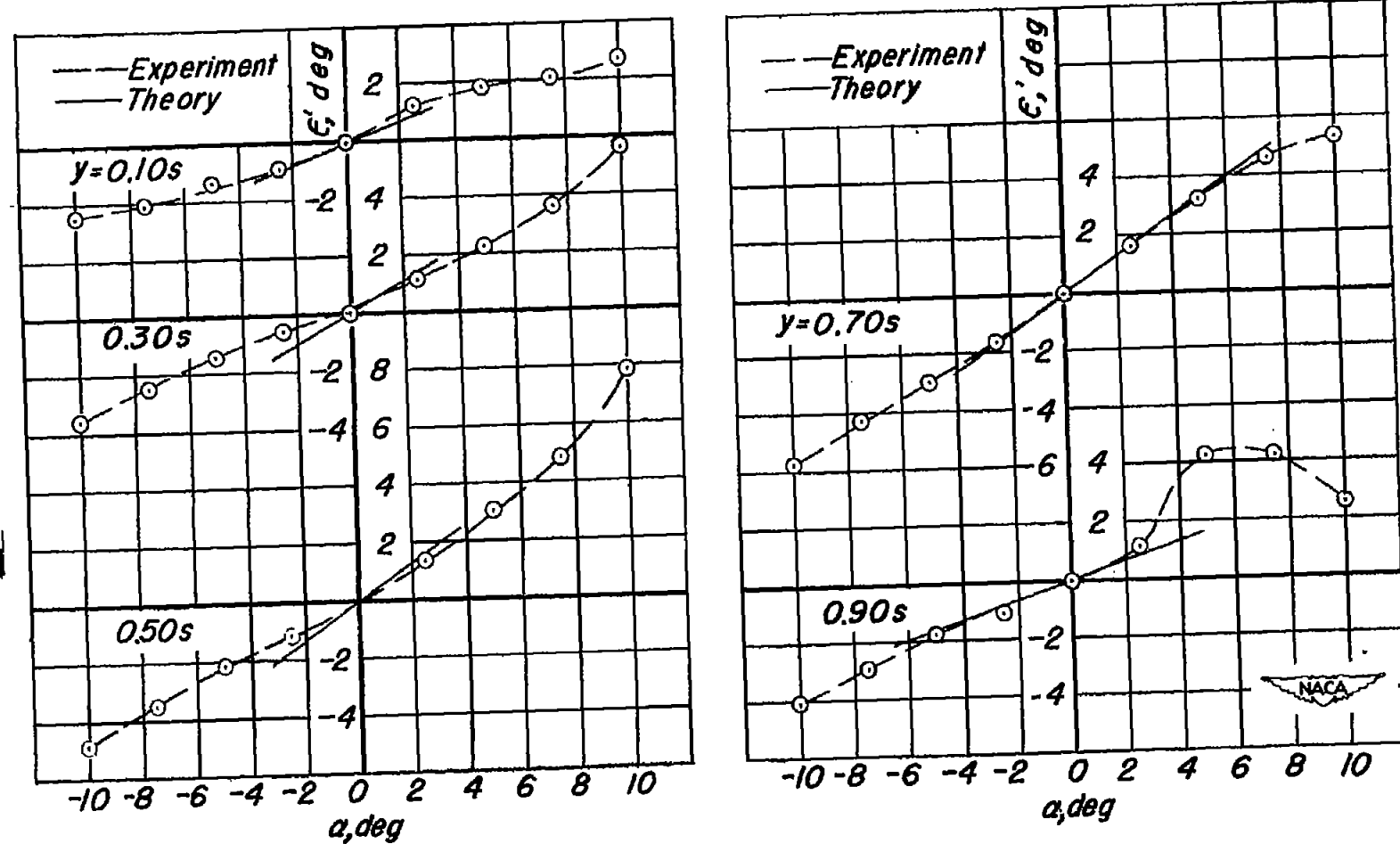
(a) Station 2, $x=1.7c$, $z=0.17c$.

Figure 5. — Variation of downwash angle with angle of attack, Model B.

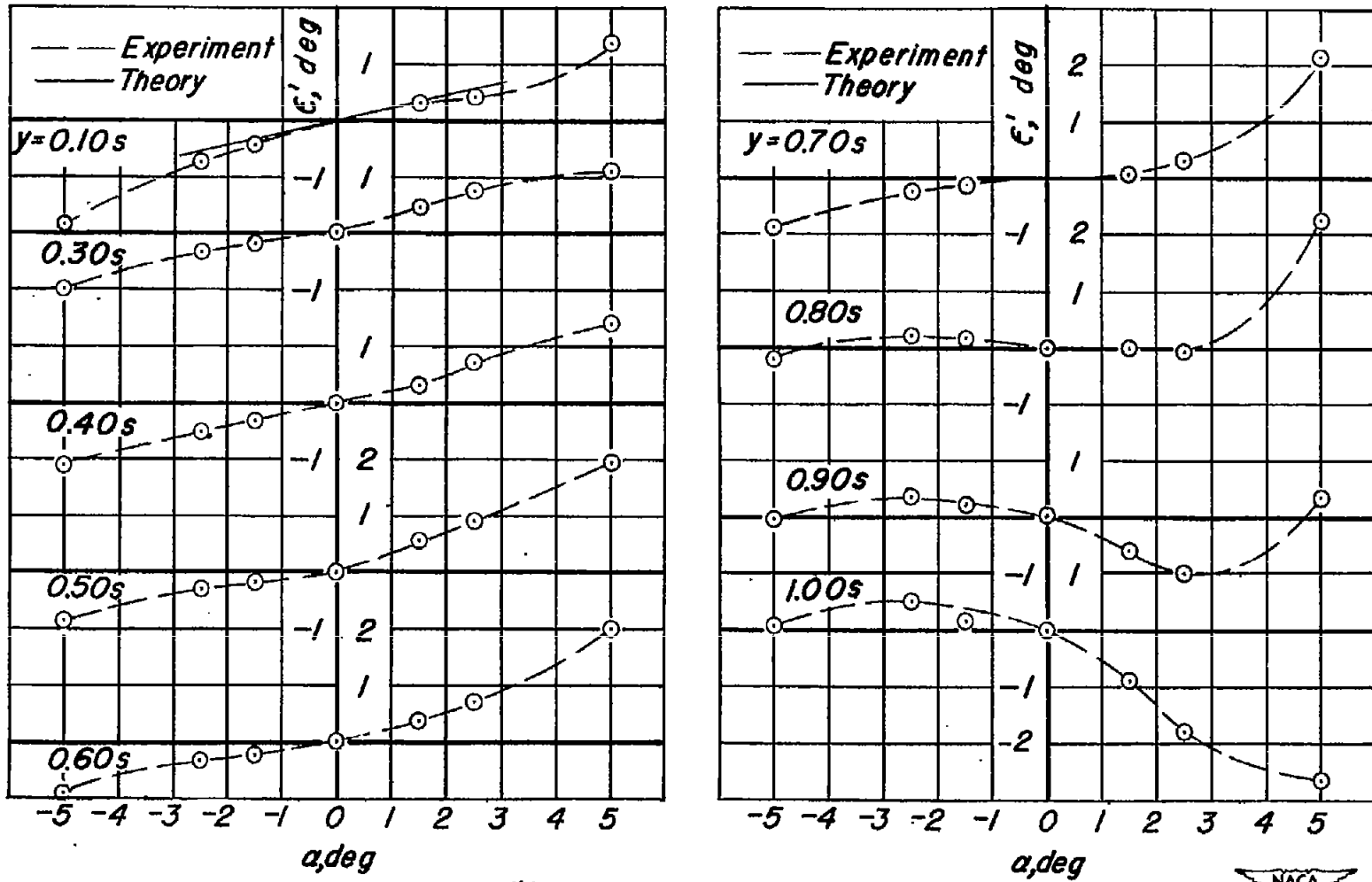
(b) Station 4, $x=2.4c, z=.17c$.

Figure 5. — Concluded.

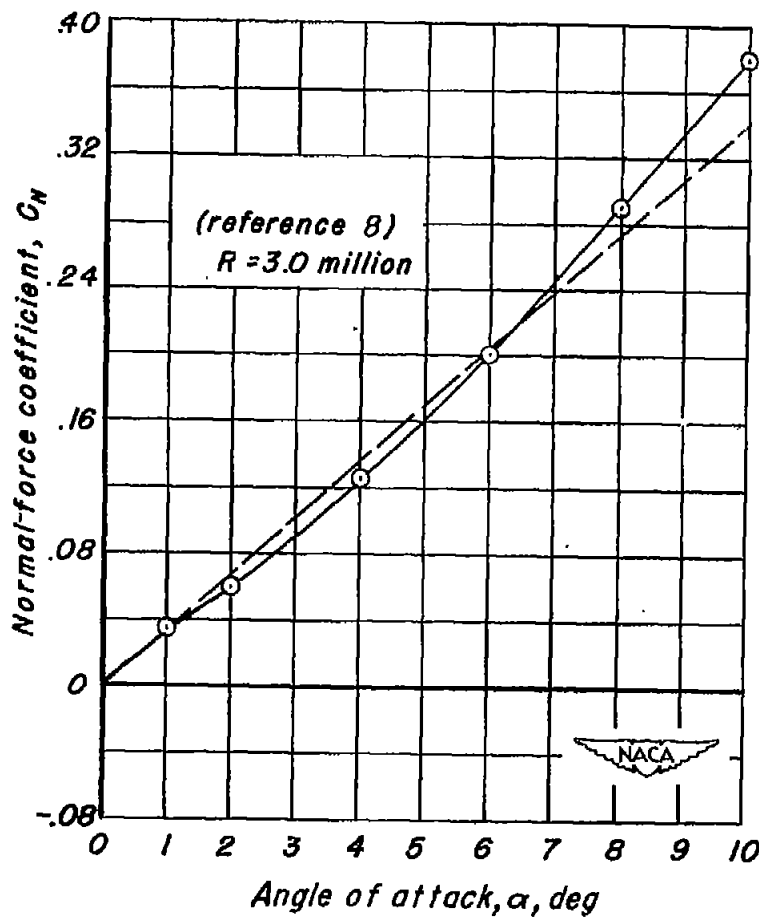
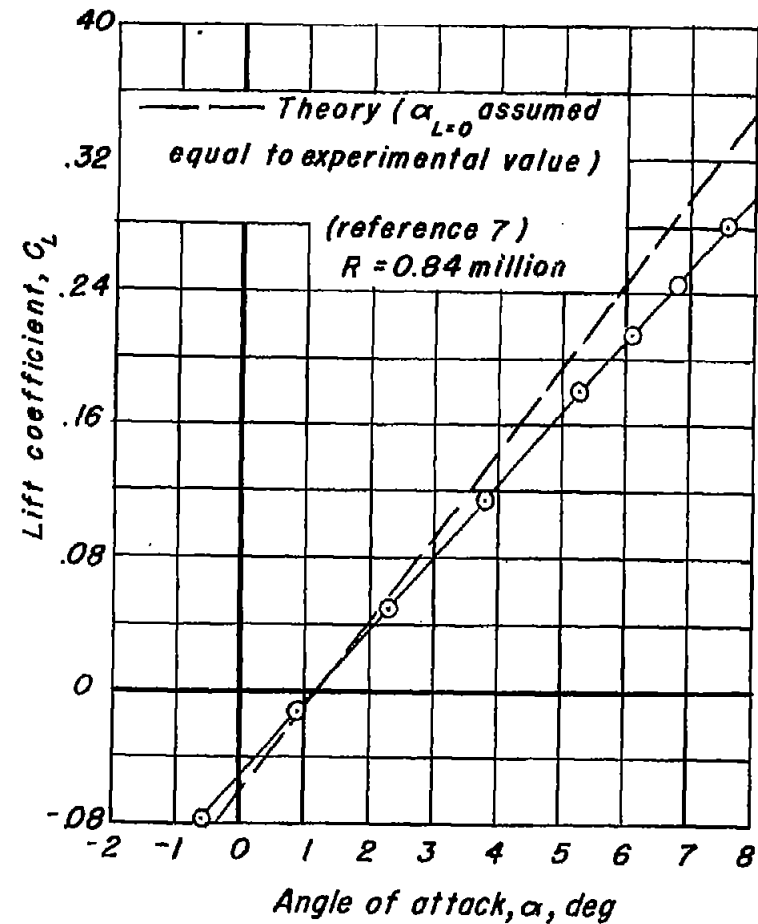
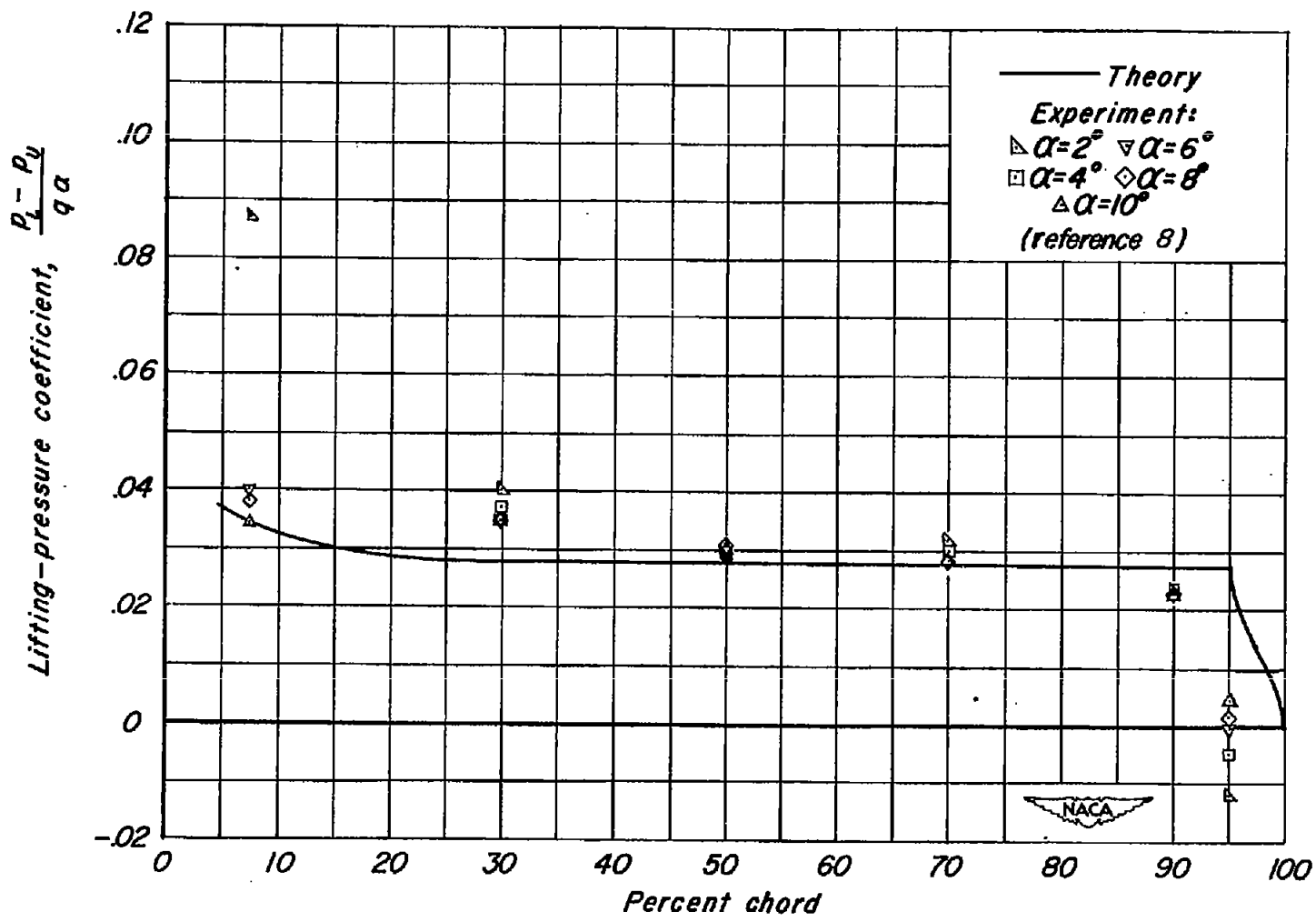
(a) Model A, lift coefficient, C_L .(b) Model B, normal-force coefficient, C_N .

Figure 6—Variation of force coefficients with angle of attack.



(a) 6.4% s.

Figure 7.— Chordwise variation of lifting-pressure coefficient per degree angle of attack at several angles of attack at five spanwise stations; $R = 3.0 \times 10^6$.

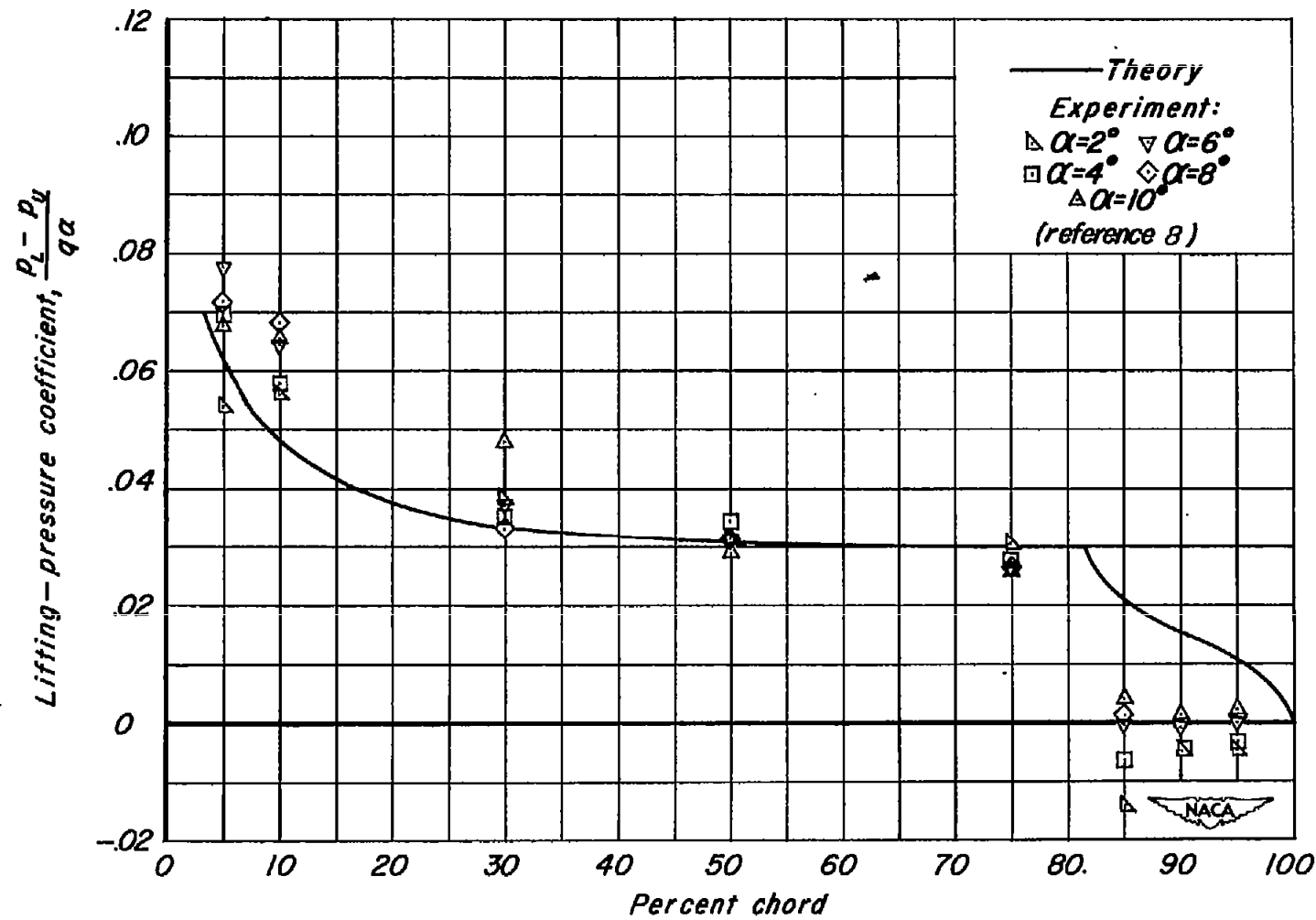
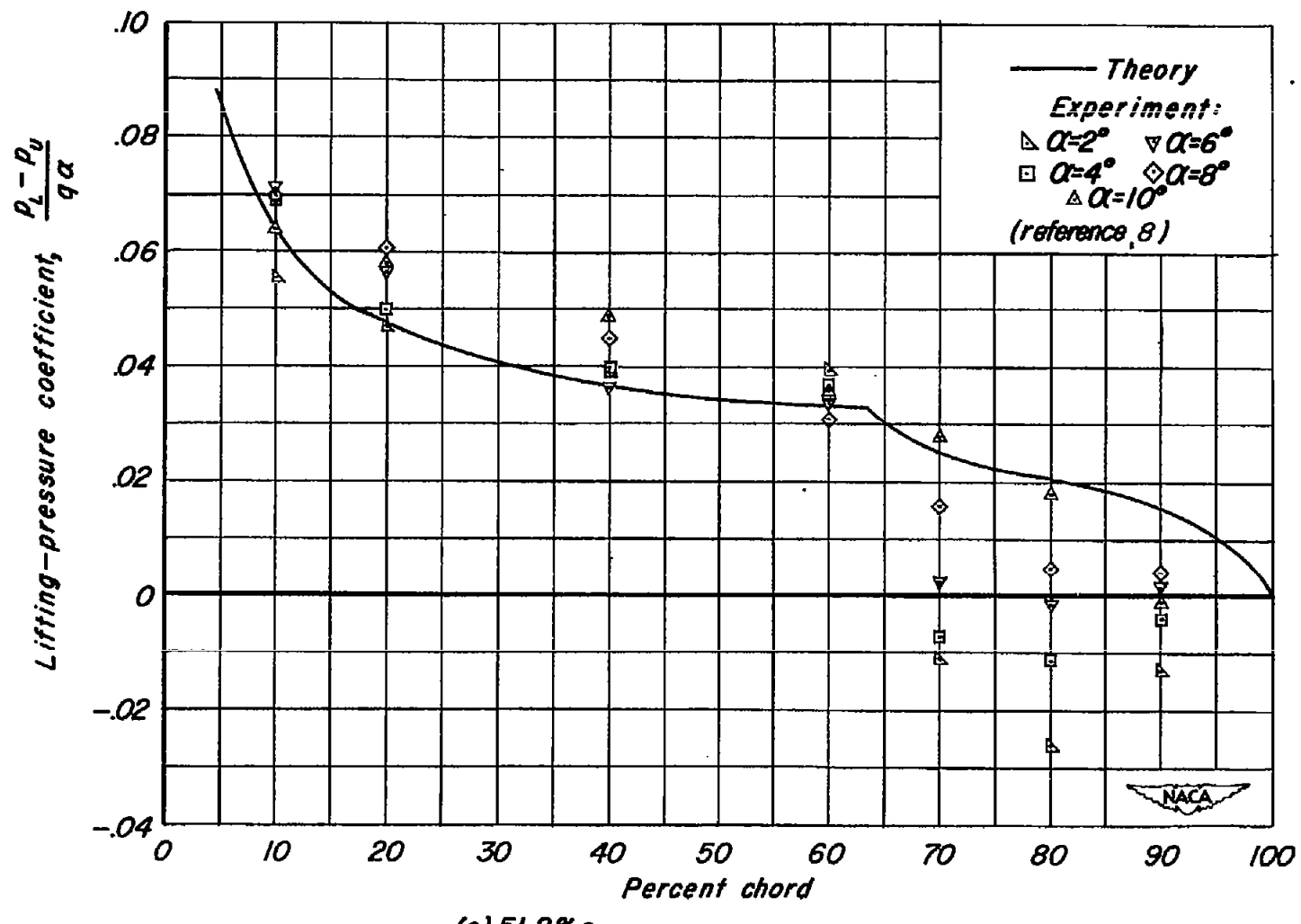


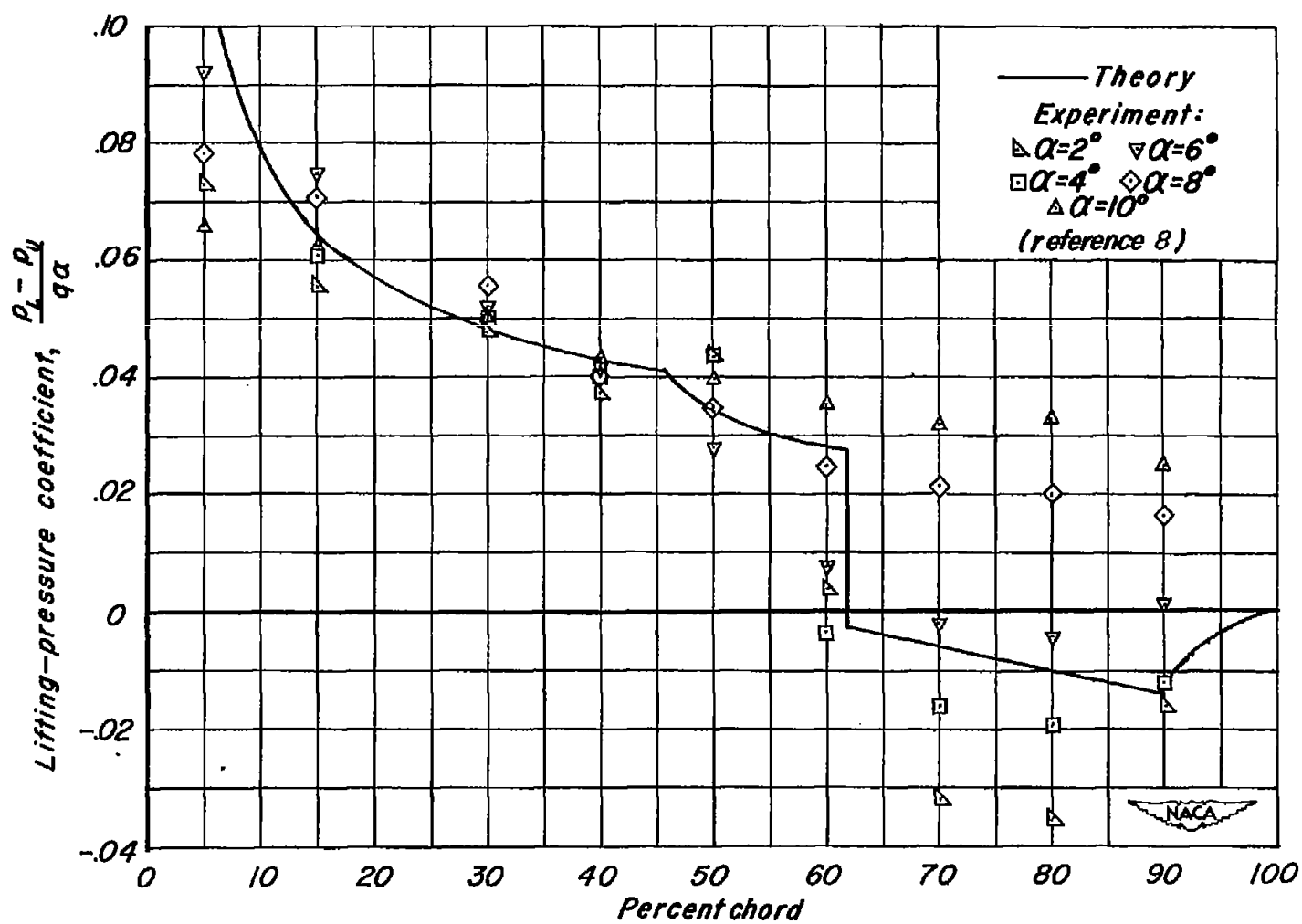
Figure 7. - Continued.

(b) 25.6% s.



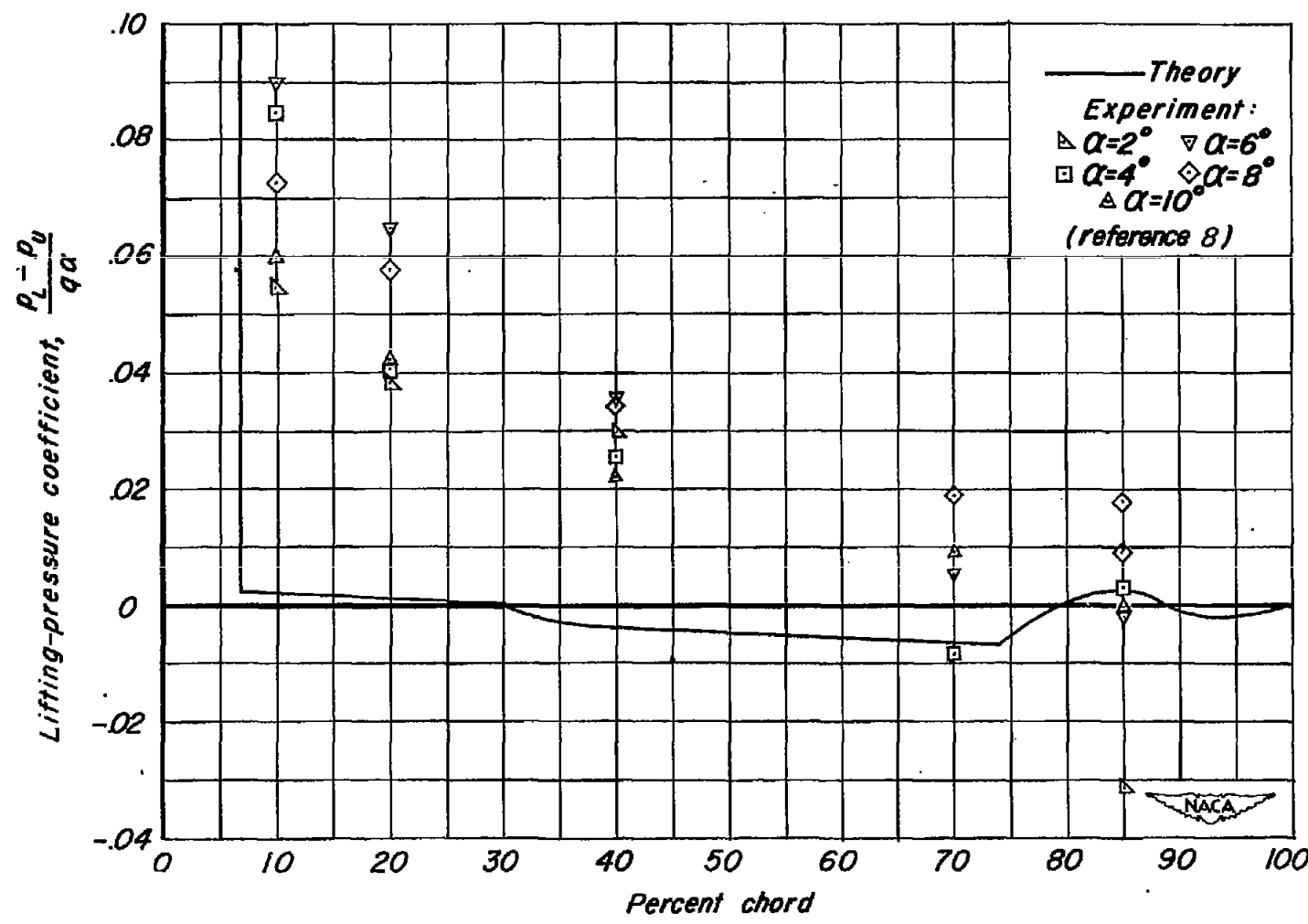
(c) 51.2% s.

Figure 7.—Continued.



(d) 76.9% s.

Figure 7.— Continued.



(e) 97.5% s.

Figure 7. Concluded.

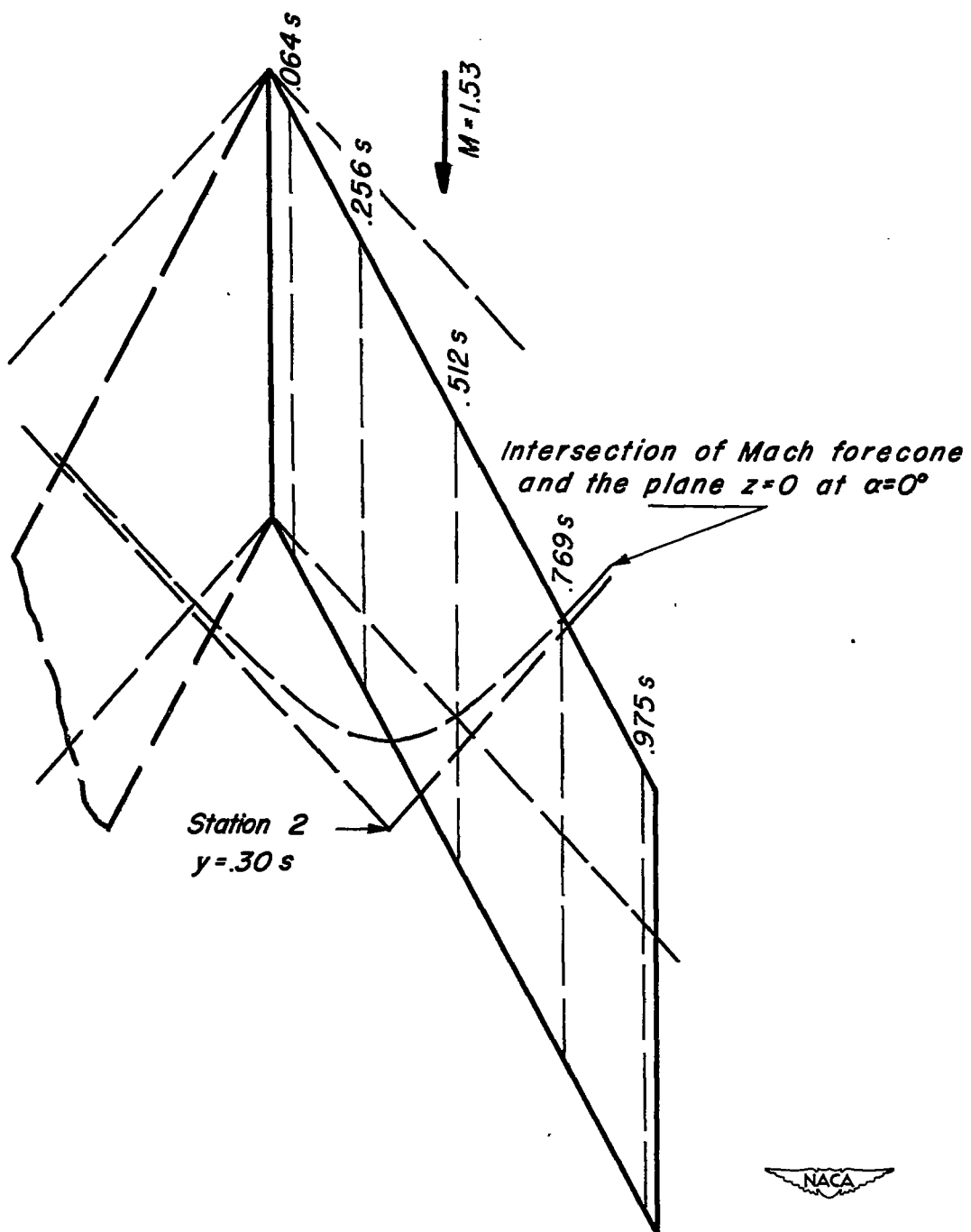


Figure 8.—Sketch of model B showing pressure-distribution stations (reference 8) and intersection of Mach forecone of the 30-percent-semispan point at station 2 and the plane of the wing at zero lift.

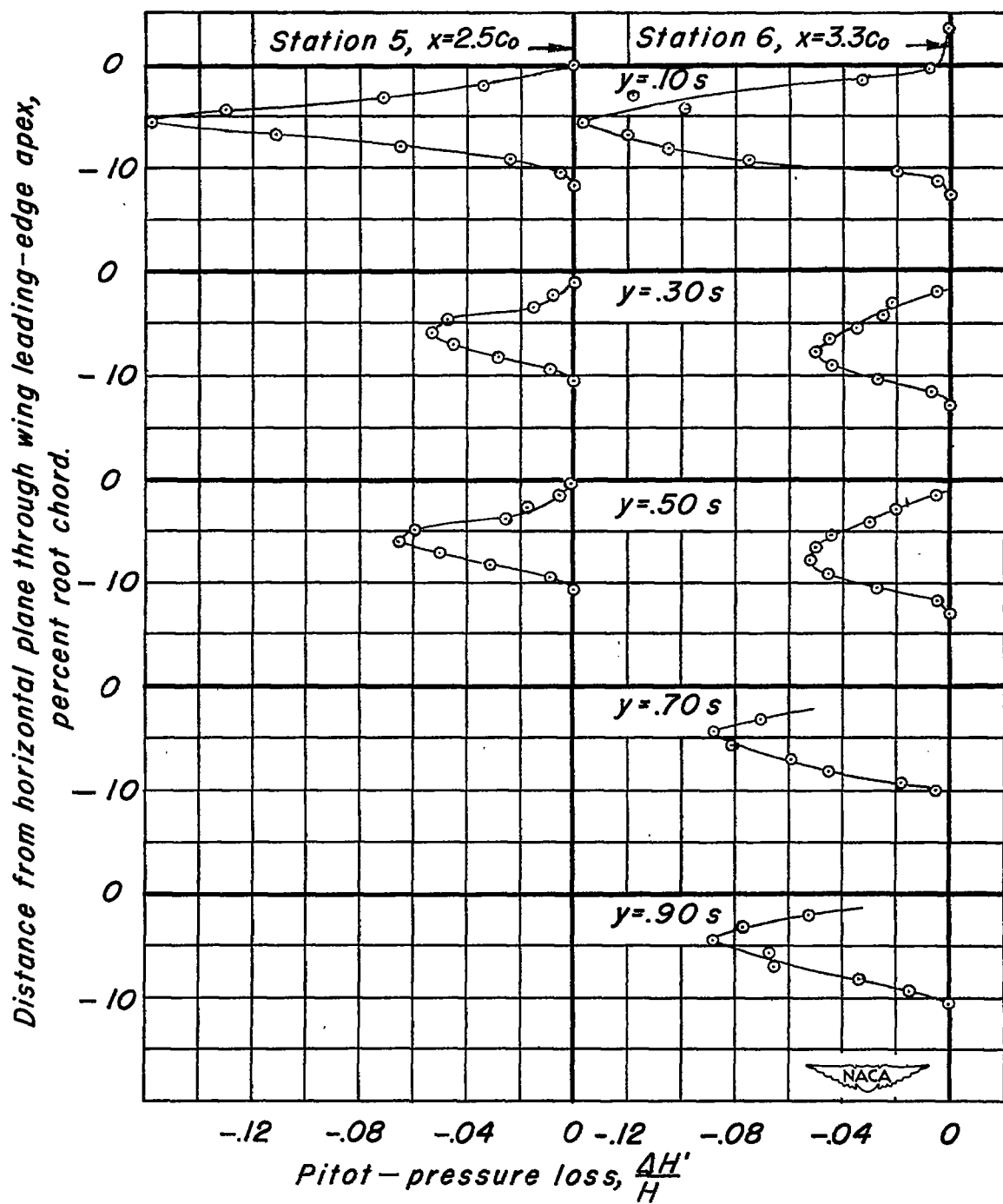


Figure 9.—Profiles of pitot-pressure loss through viscous wake of model A; $\alpha=3^\circ$.

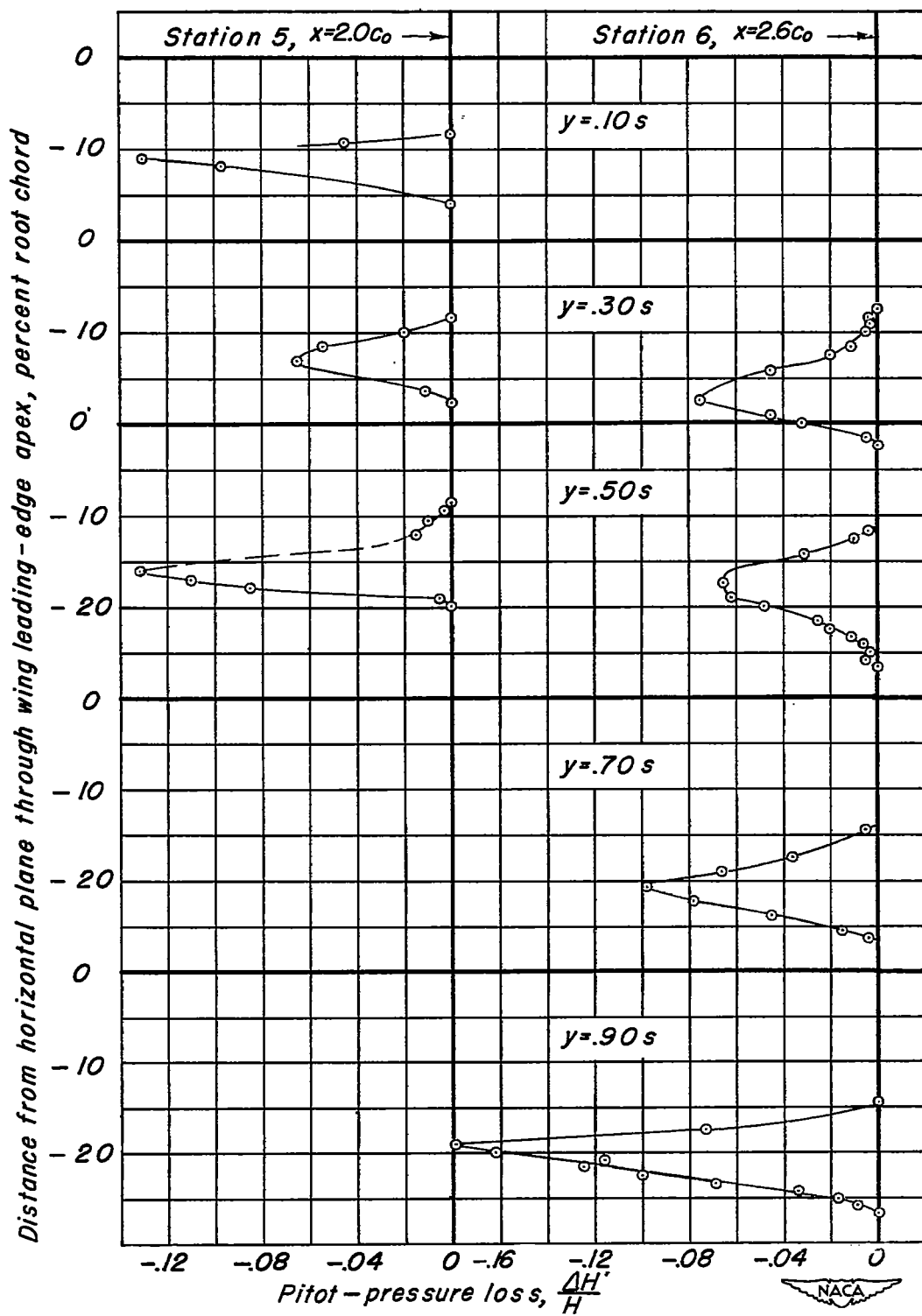


Figure 10.—Profiles of pitot-pressure loss through viscous wake of model B; $\alpha = 6^\circ$.

NACA

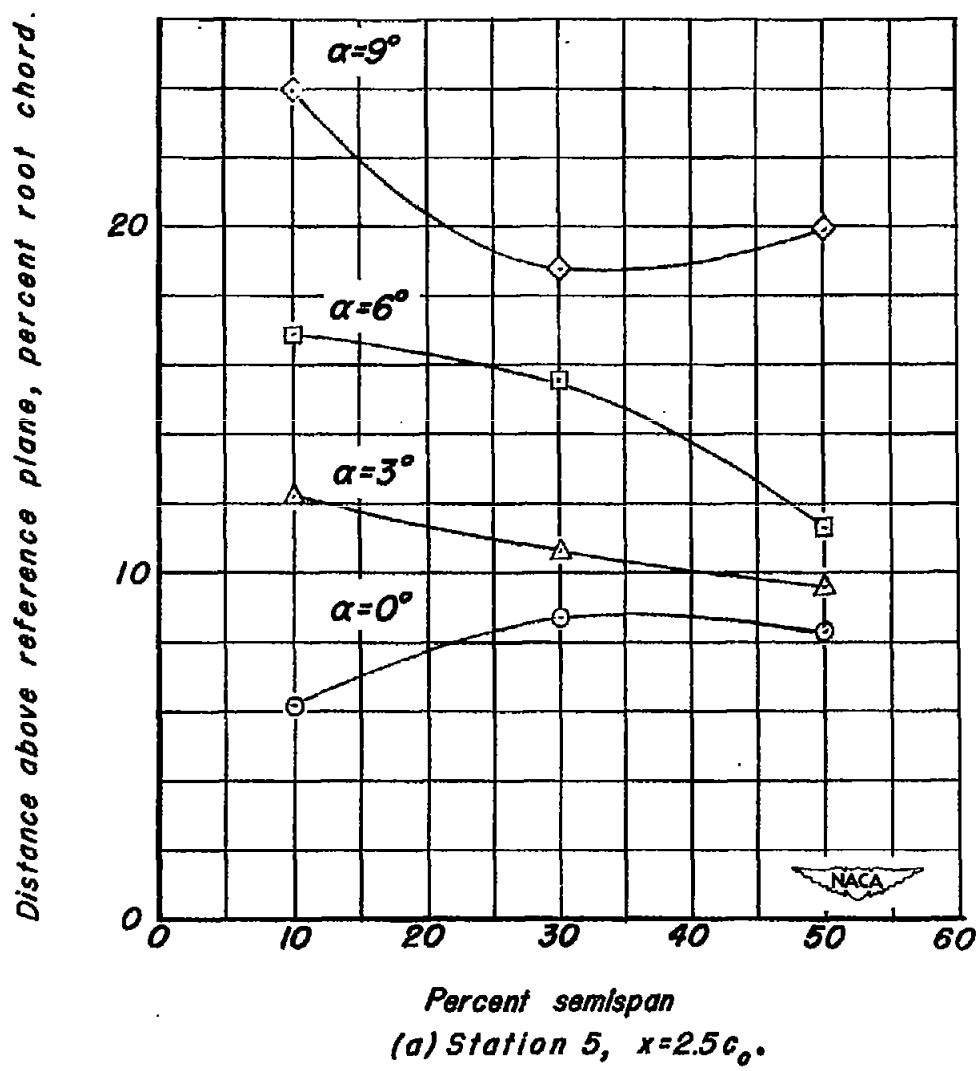


Figure II.—Position of upper limit of wake relative to plane containing the wing-leading edge and root-chord line, model A.

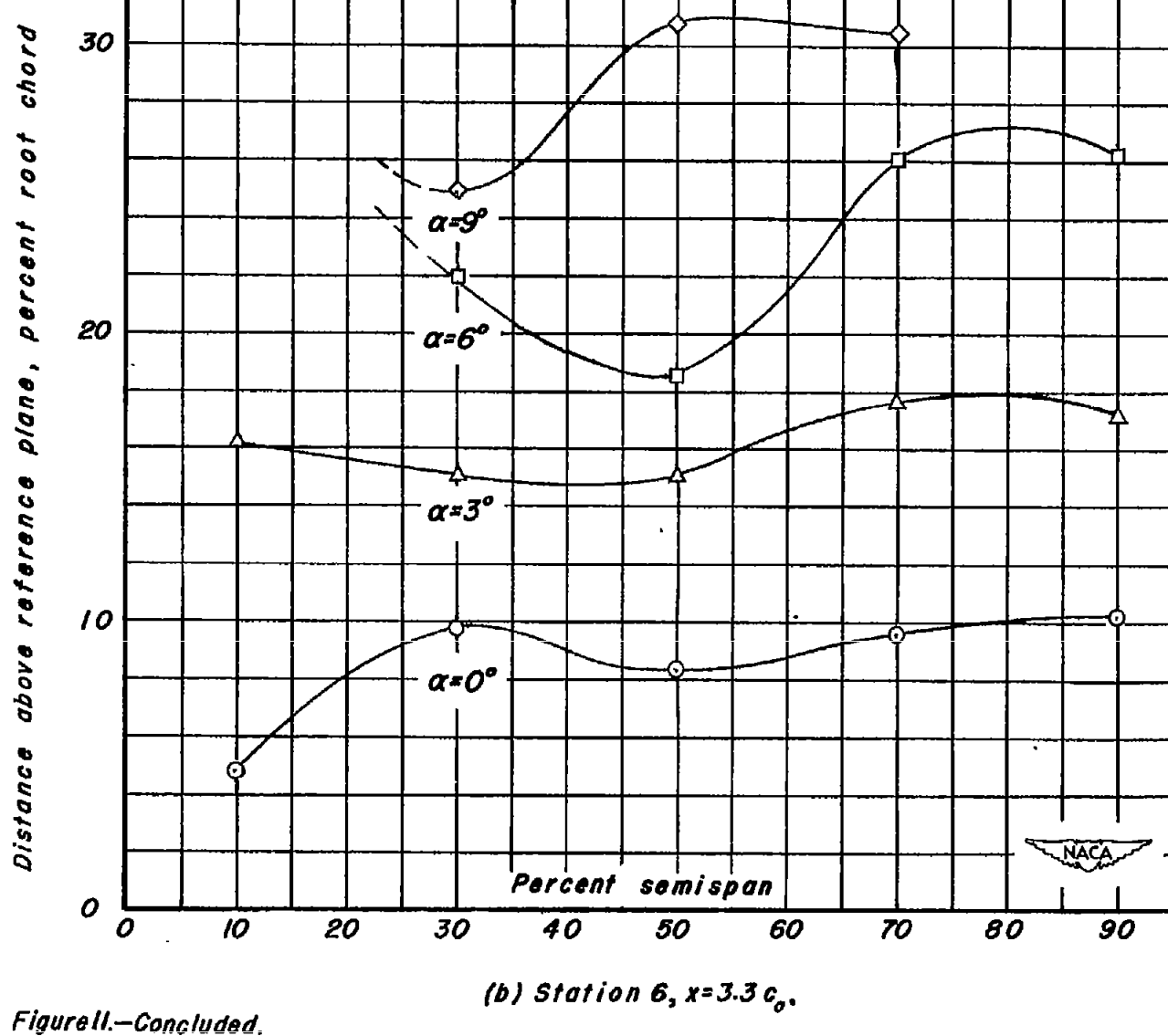


Figure II.—Concluded.

(b) Station 6, $x=3.3 c_0$.

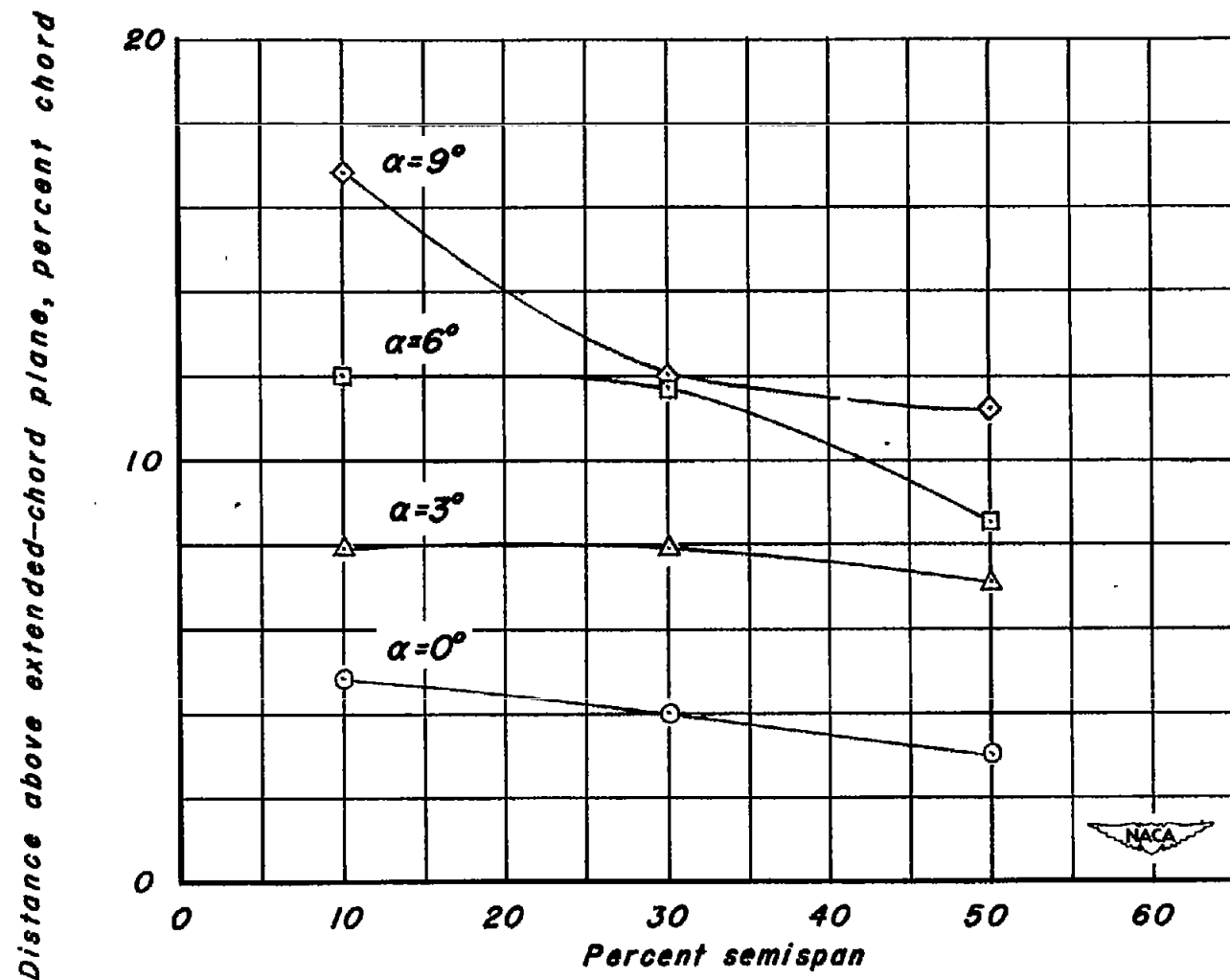
(a) Station 5, $x = 2.0 c_0$.

Figure 12—Position of upper limit of wake relative to wing-chord plane, model B.

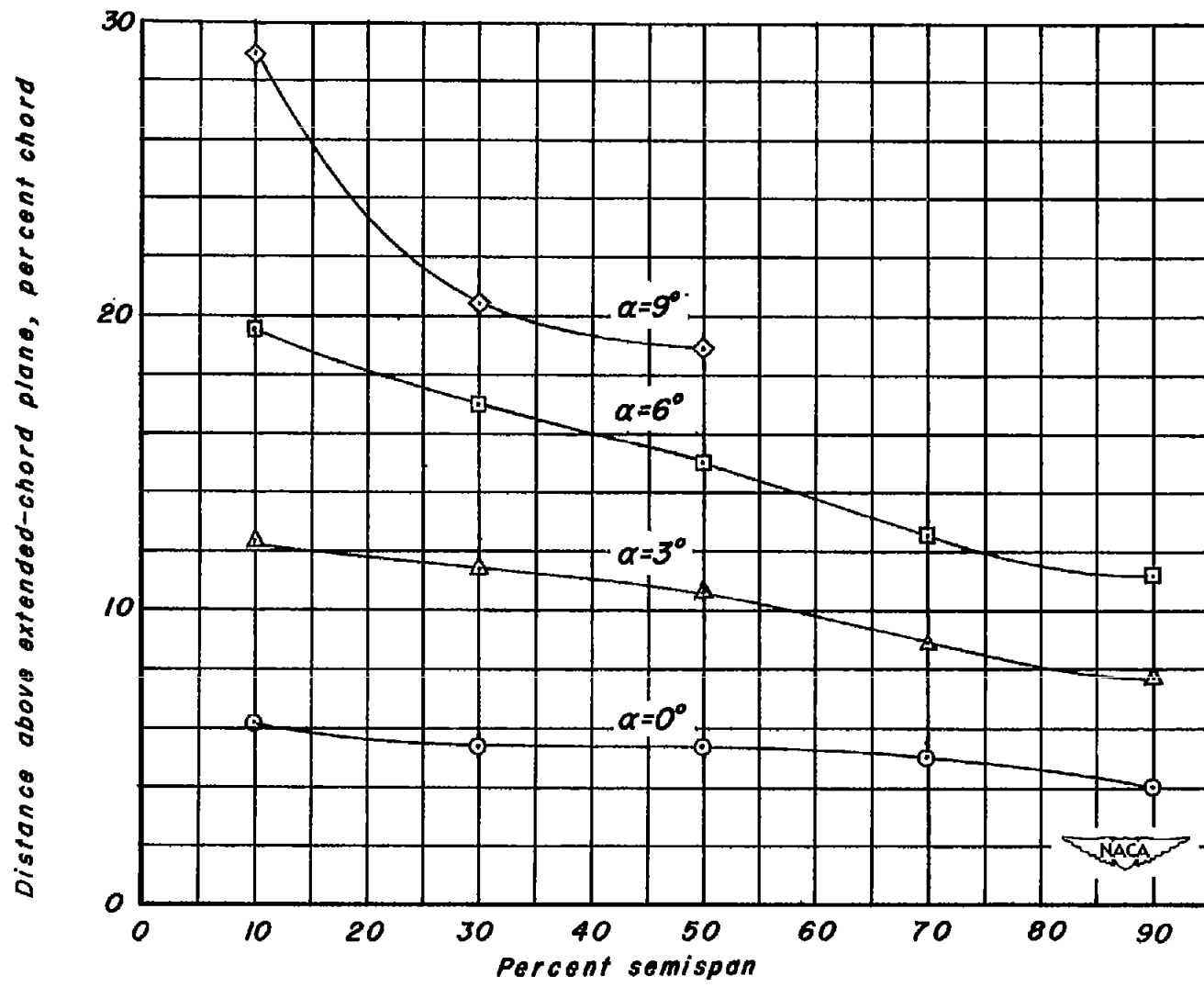
(b) Station 6, $x = 2.6 c_0$.

Figure 12—Concluded.